THE CRYSTAL STRUCTURE OF BLATTERITE, $Sb^{5+}_3(Mn^{3+},Fe^{3+})_9(Mn^{2+},Mg)_{35}(BO_3)_{16}O_{32}$, AND STRUCTURAL HIERARCHY IN Mn^{3+}-BEARING ZIGZAG BORATES

MARK A. COOPER AND FRANK C. HAWTHORNE[1]

Department of Geological Sciences, University of Manitoba, Winnipeg, Manitoba R3T 2N2

ABSTRACT

The crystal structure of blatterite, $Sb^{5+}_3(Mn^{3+},Fe^{3+})_9(Mn^{2+},Mg)_{35}(BO_3)_{16}O_{32}$, orthorhombic, *a* 37.654(8), *b* 12.615(3), *c* 6.2472(8) Å, *V* 2968(1) Å^3, space group *Pnnm*, *Z* = 2, D(calc.) = 4.25 g.cm^{-3}, has been solved by direct methods and refined to an *R* index of 4.3% based on 2713 observed reflections measured with MoKα X-radiation. The crystal used for the collection of the X-ray intensity data was analyzed by electron microprobe; the resulting composition agrees with that derived from the crystal-structure analysis. This has led to a major revision of the chemical formula. There are 31 crystallographically distinct cations in blatterite: two *Sb*-sites occupied by octahedrally coordinated Sb^{5+}, five *Mn*-sites occupied by octahedrally coordinated Mn^{3+}, nine *M*-sites occupied by octahedrally coordinated (Mn^{2+},Mg), eight *B*-sites occupied by triangularly coordinated B, and seven *X*-sites occupied by $(Mn^{2+},\square)$; five of the *X* sites are octahedrally coordinated, and two of the *X* sites are tetrahedrally coordinated. Blatterite is a member of the (3 Å) wallpaper-borate structures in which [MO_4] chains of edge-sharing octahedra extend along the *c* axis and are cross-linked by (BO_3) groups. Many of the topological features of these structures can be idealized as colorings of the regular net 3^6. There is a group of Mn^{3+}-bearing structures (fredrikssonite, orthopinakiolite, takéuchiite, blatterite, pinakiolite) that we designate as the *zigzag borates*. As indicated earlier by Takéuchi *et al.* (1978), these can be described as having three important structural motifs: *F* walls, *C* walls and *S* columns. The crystal chemistry of this group is discussed, revised chemical formulae are given for all members of the group, and an explanation is given for the extensive positional disorder associated with the *X* cations of the *C* walls in the Mn^{3+}-bearing structures.

Keywords: blatterite, crystal-structure solution, borate, zigzag borates, cation disorder, orthopinakiolite, fredrikssonite, takéuchiite.

SOMMAIRE

Nous avons résolu la structure cristalline de la blatterite, $Sb^{5+}_3(Mn^{3+},Fe^{3+})_9(Mn^{2+},Mg)_{35}(BO_3)_{16}O_{32}$, orthorhombique, *a* 37.654(8), *b* 12.615(3), *c* 6.2472(8) Å, *V* 2968(1) Å^3, groupe spatial *Pnnm*, *Z* = 2, D(calc.) = 4.25 g.cm^{-3}, par méthodes directes; l'affinement, jusqu'à un résidu *R* de 4.3%, a porté sur 2713 réflexions observées, mésurées avec rayonnement MoKα. Le cristal utilisé pour la collection des intensités en diffraction X a ensuite été analysé avec une microsonde électronique. La composition qui en résulte concorde bien avec celle qui est dérivée des résultats de l'analyse structurale. Ce travail a mené à une révision importante de la formule chimique. Il y a 31 cations cristallographiquement distincts dans la blatterite: deux sites *Sb* contiennent le Sb^{5+} en coordinence octaédrique; cinq sites *Mn* contiennent le Mn^{3+} en coordinence octaédrique, et neuf sites *M* contiennent (Mn^{2+},Mg) en coordinence octaédrique. Huit sites de *B* à coordinence trois contiennent le bore, et sept sites *X* sont peuplés par $(Mn^{2+},\square)$; de ceux-ci, cinq ont une coordinence octaédrique, et deux d'entre eux ont une coordinence tétraédrique. La blatterite

[1] *E-mail address*: frank_hawthorne@umanitoba.ca

fait partie du groupe des borates à motif de "papier peint" (3 Å) dans lesquels les chaînes [MO_4] d'octaèdres à arêtes partagées se propagent le long de l'axe c et sont interliées par des groupes (BO_3). On peut idéaliser les aspects topologiques de ces structures en considérant des schémas coloriés d'un réseau régulier 3^6. Nous traitons ici de borates en zigzag un groupe de structures contenant le Mn^{3+} (fredrikssonite, orthopinakiolite, takéuchiite, blatterite, pinakiolite). Comme l'avaient indiqué antérieurement Takéuchi *et al.* (1978), ces structures auraient trois motifs structuraux importants: des parois F, des parois C et des colonnes S. Nous traitons de la cristallochimie de ce groupe, nous proposons des formules révisées pour chaque membre, et nous justifions la présence d'un désordre de position important associé avec les cations X des parois C des structures riches en Mn^{3+}.

(Traduit par la Rédaction)

Mots-clés: blatterite, solution de la structure cristalline, borate, borates en zigzag, désordre des cations, orthopinakiolite, fredrikssonite, takéuchiite.

Introduction

Blatterite is an Sb- and Mn-bearing borate mineral discovered on the dumps of the Kittelgruvan mine, Nordmark, Värmland, Sweden, although it is believed to come from the Brattforsgruvan mine in the same orefields (Raade *et al.* 1988). Its formula was given as (Mn^{2+},Mg)$_2$ (Mn^{2+},Mn^{3+},Sb^{5+},Fe^{3+}) (BO_3) O_2, and it was assigned to the pinakiolite group on the basis of its composition and unit-cell dimensions. As part of a general study of the borate minerals (Burns & Hawthorne 1993a, b, 1994a, b, c, d, e, 1995, Burns *et al.* 1992, 1994, 1995, Cooper *et al.* 1994, Hawthorne *et al.* 1996), we have solved the structure of blatterite and discuss its relation to other Mn^{3+}-bearing wallpaper borate minerals. After the experimental work was complete, Bovin *et al.* (1996) reported the structure of what they called both "blatterite" and "a blatterite mineral"; their material is actually the un-named Mg analogue of blatterite.

Experimental

The material used in this work is from Långban, Sweden, and was generously donated by Forrest Cureton. Several wallpaper borates from the Långban locality are found as less-than-perfect contiguous crystals with incipient alteration along cleavage and parting traces, and blatterite is no exception. Raade *et al.* (1988) described precession photographs of blatterite as containing streaky and diffuse spots yielding a variable a period. As blatterite is essentially opaque, the best visual gauge of crystal quality is *via* careful rotation of a crystal in reflected light. The combination of high reflectance and fine striae provides a sensitive indicator of crystal perfection. In this manner, we selected a suitable crystal. On zero- and first-level precession photographs, there was no indication of anything other than a uniform a repeat of ~38 Å, and all reflections are circular and uniformly sharp. The crystal was mounted on a Siemens $P4$ automated four-circle single-crystal diffractometer equipped with a Mo-target X-ray tube and a highly oriented graphite-crystal monochromator mounted in equatorial geometry. The crystal was

aligned on all Laue equivalents of eleven h k l values with $15 < 2\theta < 55°$, a total of forty reflections in all; the resulting unit-cell dimensions are given in Table 1. The scan range for each reflection was reduced as much as possible, the crystal–detector distance was set to the maximum value possible, and the smallest collimators were used to produce a narrow, highly collimated beam. Careful examination of the background readings in those areas of reciprocal space most prone to reflection overlap (as assessed from precession photographs) showed that the experimental conditions were sufficiently optimized that appropriate background readings were taken for all data. The minimum scan-rate for weak reflections was 1.5°2θ/min, sufficient to significantly enhance the supercell reflections to the extent that the complete structure was resolved. A total of 5324 unique reflections was collected in the range $4 < 2\theta < 75°$ with the index ranges $0 \le h \le 64$, $0 \le k \le 21$, $0 \le l \le 10$. A total of 21 psi-scan reflections was collected every 5° rotation on psi over the 2θ range of the normal intensity data, and an absorption correction, modeling the crystal as an ellipsoid, reduced R(azimuthal) from 8.5 to 3.1%.

Direct methods revealed most of the metal and anion positions for the true cell, and subsequent cycles of least-squares refinement and difference-Fourier mapping resulted in convergence to an R index of 4.3% for 2713 observed reflections. Details of the unit cell, data collection and refinement information are given in Table 1.

TABLE 1. MISCELLANEOUS INFORMATION FOR BLATTERITE

a (Å)	37.654(8)	crystal size (mm)	0.06 x 0.10 x 0.16
b	12.615(3)	radiation	Mo$K\alpha$/Graphite
c	6.2472(8)	No. of intensities	5324
V (Å^3)	2968(1)	No. of $|F_o| > 5\sigma |F_o|$	2713
Sp. Gr.	$Pnnm$	R(azimuthal) %	8.5 → 3.1
mμ (mm^{-1})	7.75	R(obs) %	4.3
D_c (g.cm^{-3})	4.25	wR(obs) %	4.3

Cell content: 2[$Sb^{5+}_{5.01}$ ($Mn^{3+}_{1.73}Fe^{3+}_{0.93}Al_{0.26}Ti_{0.09})_{\Sigma 3}$ ($Mn^{2+}_{20.87}Mg_{14.06})_{\Sigma 34.93}$ (BO_3)$_{16}$ O_{32}]

$R = \Sigma(|F_o|-|F_c|)/\Sigma|F_o|$

$wR = [\Sigma w(|F_o|-|F_c|)^2/\Sigma F_o^2]^{1/2}$, $w = 1$

TABLE 2. FINAL ATOMIC PARAMETERS AND DISPLACEMENT FACTORS ($U_{ij} \times 10^4$) FOR BLATTERITE

	x	y	z	U_{eq}	U_{11}	U_{22}	U_{33}	U_{23}	U_{13}	U_{12}
Sb(1)	0	0	0	60(3)	63(5)	55(5)	62(5)	0	0	12(4)
Sb(2)	0.37486(2)	0.28738(7)	1/2	66(2)	66(4)	58(3)	75(3)	0	0	−4(3)
Mn(1)	0	1/2	0	61(7)	54(12)	62(12)	66(12)	0	0	5(9)
Mn(2)	0.25239(5)	0.0645(2)	0	69(5)	55(9)	86(10)	67(8)	0	0	−3(6)
Mn(3)	0.06329(5)	0.3952(2)	0	69(5)	76(8)	50(7)	81(8)	0	0	12(6)
Mn(4)	0.18948(5)	0.1832(2)	0	74(5)	89(9)	64(8)	70(8)	0	0	16(6)
Mn(5)	0.12551(5)	0.2853(2)	0	68(5)	43(8)	86(9)	77(8)	0	0	22(7)
M(1)	0.25299(5)	0.0646(2)	1/2	103(6)	114(9)	106(11)	89(9)	0	0	−38(7)
M(2)	1/2	1/2	0	87(11)	88(19)	95(19)	77(18)	0	0	−10(14)
M(3)	0.37460(6)	0.2875(2)	0	79(6)	70(12)	92(11)	74(10)	0	0	−24(9)
M(4)	0.18903(4)	0.4059(1)	0.2513(3)	84(4)	101(7)	62(6)	89(6)	7(7)	−4(7)	−10(5)
M(5)	0.06157(4)	0.1724(1)	0.2499(4)	80(5)	79(8)	64(8)	98(8)	−3(8)	−6(8)	−9(5)
M(6)	0.31388(5)	0.4598(1)	0.2535(3)	89(4)	100(8)	75(7)	91(8)	−8(8)	−5(8)	8(5)
M(7)	0.43639(4)	0.1159(1)	0.2478(3)	84(4)	84(7)	74(7)	96(7)	8(8)	5(8)	16(5)
M(8)	0.31042(5)	0.1827(1)	0.2438(4)	76(5)	66(9)	77(8)	85(8)	1(8)	3(8)	−8(5)
M(9)	0.43673(6)	0.3959(2)	0.2413(4)	76(5)	80(10)	64(9)	84(10)	−3(11)	−7(10)	−12(6)
X(1)	0.1874(3)	0.1799(3)	1/2	98(11)*	138(32)	61(9)	94(9)	0	0	−21(13)
X(2)	0.178(1)	0.187(2)	1/2	98(11)*	138(32)	61(9)	94(9)	0	0	−21(13)
X(3)	0.1207(1)	0.3019(4)	1/2	190(11)	225(18)	275(24)	70(11)	0	0	−197(17)
X(4)	0.0274(4)	0.4086(7)	1/2	268(32)	533(85)	203(35)	69(22)	0	0	−186(43)
X(5)	0.0526(4)	0.3994(5)	1/2	294(33)	708(93)	87(26)	86(24)	0	0	15(32)
X(6)	0.1036(6)	0.368(2)	1/2	353(68)	540(138)	498(145)	21(45)	0	0	−489(124)
X(7)	0.0092(8)	0.469(3)	1/2	372(134)	273(160)	768(384)	74(65)	0	0	−455(190)
B(1)	0.4914(2)	0.2568(5)	0	69(5)*						
B(2)	0.4928(2)	0.2566(5)	1/2	69(5)*						
B(3)	0.3677(2)	0.0440(5)	1/2	69(5)*						
B(4)	0.3682(2)	0.0426(5)	0	69(5)*						
B(5)	0.2587(2)	0.3295(5)	0	69(5)*						
B(6)	0.2559(2)	0.3202(5)	1/2	69(5)*						
B(7)	0.1181(2)	0.0313(5)	0	69(5)*						
B(8)	0.1172(2)	0.0397(5)	· 1/2	69(5)*						
O(1)	0.2764(3)	0.2345(6)	0	136(20)						
O(2)	0.2748(2)	0.2274(6)	1/2	86(17)						
O(3)	0.3508(3)	−0.0529(6)	0	130(20)						
O(4)	0.3484(2)	−0.0481(6)	1/2	86(17)						
O(5)	0.0989(2)	0.1337(6)	1/2	98(17)						
O(6)	0.0987(2)	0.1233(6)	0	109(19)						
O(7)	0.2195(2)	0.3212(7)	1/2	71(16)						
O(8)	0.2224(2)	0.3342(7)	0	95(18)						
O(9)	0.0986(2)	−0.0538(6)	1/2	81(16)						
O(10)	0.1003(2)	−0.0635(6)	0	84(16)						
O(11)	0.5278(2)	0.2587(8)	0	101(18)						
O(12)	0.5292(2)	0.2555(8)	1/2	98(18)						
O(13)	0.1544(2)	0.0312(8)	0	101(18)						
O(14)	0.1535(2)	0.0377(8)	1/2	95(17)						
O(15)	0.4046(2)	0.0445(8)	0	119(20)						
O(16)	0.4041(2)	0.0446(8)	1/2	106(19)						
O(17)	0.3415(4)	0.3213(4)	0.269(1)	53(10)						
O(18)	0.4089(1)	0.2570(4)	0.269(1)	58(9)						
O(19)	0.2747(2)	0.4132(6)	1/2	101(17)						
O(20)	0.2784(2)	0.4209(6)	0	81(16)						
O(21)	0.1606(2)	0.2549(5)	0.218(1)	88(11)						
O(22)	0.3498(2)	0.1363(6)	0	92(17)						
O(23)	0.3503(2)	0.1393(6)	1/2	100(17)						
O(24)	0.0900(2)	0.3203(5)	0.212(1)	89(11)						
O(25)	0.2843(1)	0.0422(4)	0.230(1)	70(10)						
O(26)	0.0352(2)	0.4679(5)	0.209(1)	87(11)						
O(27)	0.4724(2)	0.3493(6)	0	86(17)						
O(28)	0.4755(2)	0.3522(6)	1/2	77(16)						
O(29)	0.0336(2)	0.0329(4)	0.231(1)	77(10)						
O(30)	0.2147(2)	0.1066(5)	0.219(1)	88(11)						
O(31)	0.4735(2)	0.1645(6)	1/2	94(18)						
O(32)	0.4742(3)	0.1611(6)	0	139(21)						

*constrained to be equal.

Final atom positions and displacement factors are given in Table 2, refined and assigned site-occupancies are given in Table 3, selected interatomic distances are listed in Table 4, and a bond-valence table is shown as Table 5. Structure-factor tables can be obtained from The Depository of Unpublished Data, CISTI, National Research Council, Ottawa, Ontario K1A 0S2.

The crystal used for collection of the X-ray intensity data was then analyzed with an electron microprobe using a Cameca SX–50 operating in wavelength-disper-sion mode at 15 kV and 5 nA. The following standards were used: Mg: forsterite, Mn: spessartine, Al: kyanite, Fe: fayalite, Ti: titanite, Sb: Sb_2O_3; the amount of B_2O_3 was calculated from the crystal structure (Hawthorne & Grice 1990); the ratio Mn_2O_3: MnO was calculated for electroneutrality, and Fe was assumed to be in the triva-lent state (as in other minerals of this group). The count times for all element peak and background determi-nations were 20 and 10 s, respectively. The analytical data were reduced and corrected using the $\phi(\rho z)$ method

TABLE 3. SITE OCCUPANCIES FOR BLATTERITE

	Multiplicity	Sb^{5+}	Mn^{3+}	Al	Mn^{2+}	Mg	Unit*
Sb(1)	2	1.00					F
Sb(2)	4	1.00					F
Mn(1)	2		0.90(2)	0.10(2)			C
Mn(2)	4		1.00				F,C
Mn(3)	4		0.91(2)	0.09(2)			C
Mn(4)	4		1.00				C
Mn(5)	4		1.00				C
M(1)	4				1.00(2)		C,F
M(2)	2				0.52(2)	0.48(2)	F
M(3)	4				0.62(2)	0.38(2)	F
M(4)	8				0.69(1)	0.31(1)	S
M(5)	8				0.52(1)	0.48(1)	S
M(6)	8				0.50(1)	0.50(1)	S
M(7)	8				0.58(1)	0.42(1)	S
M(8)	8				0.41(1)	0.59(1)	F
M(9)	8				0.21(1)	0.79(1)	F
X(1)	4				0.86(4)		C
X(2)	4				0.14(4)		C
X(3)	4				0.80(1)		C
X(4)	4				0.46(2)		C
X(5)	4				0.42(2)		C
X(6)	4				0.18(2)		C
X(7)	4				0.14(2)		C

*denotes the part of the structural unit (F wall, C wall, S column) to which each site belongs.

TABLE 4. SELECTED INTERATOMIC DISTANCES (Å) FOR BLATTERITE

Sb(1)–O(28)a,l	2.080(7)	x2	M(1)–O(2)	2.212(8)	
Sb(1)–O(29),e,m,n	1.965(6)	x4	M(1)–O(20)a	2.165(8)	
<Sb(1)–O>	2.003		M(1)–O(25),d	2.075(6)	x2
			M(1)–O(30),d	2.334(6)	x2
Sb(2)–O(10)c	2.101(8)		<M(1)–O>	2.199	
Sb(2)–O(17),d	1.961(6)	x2			
Sb(2)–O(18),d	1.967(6)	x2			
Sb(2)–O(23)	2.085(8)		M(2)–O(27),k	2.167(8)	x2
<Sb(2)–O>	2.007		M(2)–O(29)b,c,f,o	2.142(6)	x4
			<M(2)–O>	2.150	
Mn(1)–O(26),e,g,l	1.903(6)	x4			
Mn(1)–O(31)c,l	2.303(8)	x2			
<Mn(1)–O>	2.036				
			M(3)–O(9)c	2.242(8)	
Mn(2)–O(1)	2.328(8)		M(3)–O(17),e	2.136(6)	x2
Mn(2)–O(19)a	2.165(8)		M(3)–O(18),e	2.155(6)	x2
Mn(2)–O(25),e	1.895(6)	x2	M(3)–O(22)	2.123(8)	
Mn(2)–O(30),e	2.039(6)	x2	<M(3)–O>	2.158	
<Mn(2)–O>	2.060				
Mn(3)–O(12)l	2.294(9)				
Mn(3)–O(16)c	2.250(9)		M(4)–O(3)c	2.220(7)	
Mn(3)–O(24),e	1.913(6)	x2	M(4)–O(4)c	2.189(6)	
Mn(3)–O(26),e	1.913(6)	x2	M(4)–O(7)	2.208(6)	
<Mn(3)–O>	2.033		M(4)–O(8)	2.204(6)	
			M(4)–O(21)	2.194(8)	
Mn(4)–O(8)	2.273(9)		M(4)–O(25)f	1.995(6)	
Mn(4)–O(13)	2.327(9)		<M(4)–O>	2.168	
Mn(4)–O(21),e	1.963(6)	x2			
Mn(4)–O(30),e	1.924(6)	x2			
<Mn(4)–O>	2.062				
			M(5)–O(5)	2.158(6)	
Mn(5)–O(4)c	2.319(8)		M(5)–O(6)	2.185(6)	
Mn(5)–O(6)	2.279(8)		M(5)–O(11)l	2.194(6)	
Mn(5)–O(21),e	1.937(6)	x2	M(5)–O(12)l	2.180(6)	
Mn(5)–O(24),e	1.934(6)	x2	M(5)–O(24)	2.165(6)	
<Mn(5)–O>	2.057		M(5)–O(29)	2.054(6)	
			<M(5)–O>	2.156	
B(1)–O(11)	1.37(1)				
B(1)–O(27)	1.37(1)				
B(1)–O(32)	1.37(1)		M(6)–O(13)c	2.146(6)	
<B(1)–O>	1.37		M(6)–O(14)c	2.231(6)	
			M(6)–O(17)	2.035(5)	
B(2)–O(12)	1.37(1)		M(6)–O(19)	2.212(6)	
B(2)–O(28)	1.37(1)		M(6)–O(20)	2.129(6)	
B(2)–O(31)	1.37(1)		M(6)–O(30)f	2.150(6)	
<B(2)–O>	1.37		<M(6)–O>	2.151	
B(3)–O(4)	1.37(1)				
B(3)–O(16)	1.37(1)				
B(3)–O(23)	1.37(1)		M(7)–O(15)	2.155(6)	
<B(3)–O>	1.37		M(7)–O(16)	2.183(6)	
			M(7)–O(18)	2.064(6)	
B(4)–O(3)	1.37(1)		M(7)–O(26)l	2.168(6)	
B(4)–O(15)	1.37(1)		M(7)–O(31)	2.194(6)	
B(4)–O(22)	1.37(1)		M(7)–O(32)	2.178(7)	
<B(4)–O>	1.37		<M(7)–O>	2.157	
B(5)–O(1)	1.37(1)				
B(5)–O(8)	1.37(1)		M(8)–O(1)	2.096(7)	
B(5)–O(20)	1.37(1)		M(8)–O(2)	2.162(6)	
<B(5)–O>	1.37		M(8)–O(17)	2.109(5)	
			M(8)–O(22)	2.205(7)	
B(6)–O(2)	1.37(1)		M(8)–O(23)	2.261(6)	
B(6)–O(7)	1.37(1)		M(8)–O(25)	2.029(6)	
B(6)–O(19)	1.37(1)		<M(8)–O>	2.144	

(Pouchou & Pichoir 1984, 1985). The chemical composition (mean of 8 point determinations) and formula unit, calculated on the basis of 80 O-atoms, are listed in Table 6.

DESCRIPTION OF THE STRUCTURE

The cation sites

There are 31 crystallographically distinct cation-sites in blatterite (Table 2). Site occupancies were assigned by inspection of refined site-scattering values and consideration of the local stereochemistry. For those sites that are clearly occupied by a single scattering species, the occupancies were fixed at unity in the later cycles of refinement. Thus the *Sb* sites are occupied exclusively by Sb, and this is in accord with the chemical composition of the crystal (Table 6). The *Mn* sites are occupied by Mn, Fe and Al, whereas the *M*(1–9) sites are occupied by Mn and Mg. Summing the amount of Mg at the *M* sites as indicated by the site-scattering refinement gives 13.6(3) Mg atoms per formula unit, *apfu*; the electron-microprobe data (Table 6) indicates 14.1(1) Mg *apfu*. These values are statistically the same, and all Mg in this crystal of blatterite is considered to occur at the *M* sites. Hence the *X* sites are occupied by Mn only, and these sites are only partly filled [*i.e.*, they are also "occupied" by □ (vacancy) as well as by Mn].

Table 4 cont.

B(7)–O(6)	1.37(1)		
B(7)–O(10)	1.37(1)		
B(7)–O(13)	1.37(1)	M(9)–O(9)c	2.109(6)
<B(7)–O>	1.37	M(9)–O(10)c	2.195(6)
		M(9)–O(18)	2.048(6)
B(8)–O(5)	1.37(1)	M(9)–O(27)	2.102(6)
B(8)–O(9)	1.37(1)	M(9)–O(28)	2.247(6)
B(8)–O(14)	1.37(1)	M(9)–O(29)f	2.066(6)
<B(8)–O>	1.37	<M(9)–O>	2.128
X(1)–O(7)	2.153(11)	X(5)–O(11)l	2.203(12)
X(1)–O(14)	2.202(12)	X(5)–O(15)c	2.439(14)
X(1)–O(21),d	2.240(8) x2	X(5)–O(24),d	2.492(10) x2
X(1)–O(30),d	2.237(8) x2	X(5)–O(26),d	2.119(8) x2
<X(1)–O>	2.218	<X(5)–O>	2.311
X(2)–O(7)	2.315(39)	X(7)–O(26),d	2.067(15) x2
X(2)–O(14)	2.090(32)	X(7)–O(26)h,i	2.598(24) x2
X(2)–O(21),d	2.059(19) x2	X(7)–O(32)c	2.507(43)
X(2)–O(30),d	2.468(30) x2	X(7)–O(32)l	2.103(39)
<X(2)–O>	2.243	<X(7)–O>	2.323
X(3)–O(3)c	2.125(10)		
X(3)–O(5)	2.274(9)		
X(3)–O(21),d	2.392(7) x2		
X(3)–O(24),d	2.149(7) x2		
<X(3)–O>	2.247		
X(4)–O(11)l	2.110(13)	X(6)–O(3)c	2.001(26)
X(4)–O(26),d	1.990(7) x2	X(6)–O(15)c	2.273(27)
X(4)–O(32)l	2.189(16)	X(6)–O(24),d	1.956(12) x2
<X(4)–O>	2.070	<X(6)–O>	2.047
X(1)–X(2)	0.39(5)	X(5)–X(7)	1.85(4)
X(2)–X(3)	2.59(4)	X(4)–X(7)	1.02(4)
X(3)–X(6)	1.03(3)	X(4)–X(7)l	2.07(4)
X(6)–X(5)	1.97(3)	X(7)–X(7)i	1.05(8)
X(5)–X(4)	0.96(2)		

Symmetry operators: a: $-x+\frac{1}{2}$, $y-\frac{1}{2}$, $z-\frac{1}{2}$; b: $x+\frac{1}{2}$, $-y+\frac{1}{2}$, $z-\frac{1}{2}$; c: $-x+\frac{1}{2}$, $y+\frac{1}{2}$, $z+\frac{1}{2}$; d: x, y, $-z+1$; e: x, y, $-z$; f: $-x+\frac{1}{2}$, $y+\frac{1}{2}$, $-z+\frac{1}{2}$; g: $-x$, $-y+1$, $-z$; h: $-x$, $-y+1$, $-z+1$; i: $-x$, $-y+1$, z; j: $-x+\frac{1}{2}$, $y-\frac{1}{2}$, $-z+\frac{1}{2}$; k: $-x+1$, $-y+1$, z; l: $x-\frac{1}{2}$, $-y+\frac{1}{2}$, $z-\frac{1}{2}$; m: $-x$, $-y$, $-z$; n: $-x$, $-y$, z; o: $x+\frac{1}{2}$, $-y+\frac{1}{2}$, $-z+\frac{1}{2}$

B–O distances constrained to be 1.37 Å

The B sites: There are eight distinct B-sites, each of which is occupied by B and is coordinated by three O-atoms in a triangular arrangement. The B sites were refined initially with an isotropic-displacement factor. This led to B–O distances that gave bond-valence sums less than 3 valence units, *vu*. The grand <B–O> was 1.384 Å, and the average incident bond-valence sum at the B sites was 2.86 *vu*. The variations in both individual (1.35–1.42 Å) and mean (1.379–1.393 Å) bond-lengths fall well within the range reported for well-refined structures of borate minerals (Hawthorne *et al.* 1996). However, in a structure refinement of this complexity, where there is significant correlation among refined parameters *and* the overall data-to-parameter ratio is small, systematic error in relation to the weaker scattering species B (5 e^-) and O (8 e^-) is likely. In order to avoid bias in the rest of the refined structure-model due to this problem, the B–O distances were constrained to be equal to 1.37 Å in the last stages of refinement.

The Sb sites: There are two distinct Sb-sites, both coordinated by six O-atoms in octahedral arrangements. The

<Sb–O> distances and the details of the coordination geometry indicate that Sb is in the pentavalent state in blatterite; this conclusion is also in accord with the electroneutrality requirements of the blatterite formula.

The Mn sites: There are five distinct Mn-sites, each of which is octahedrally coordinated by O atoms. The refined site-scattering values for the Mn(1) and Mn(3) sites are less than 25 *epfu* (electrons per formula unit), indicating that the Mn(1) and Mn(3) sites contain minor Al. Summing the amount of Al at the Mn(1) and Mn(3) sites, as indicated by the site-scattering refinement, gives 0.28(6) Al *apfu*. The electron-microprobe data (Table 6) gives 0.25(2) Al *epfu*, in good agreement with the results of the site-scattering refinement.

Both the <Mn–O> distances and the variation in individual bond-lengths at each site show that the constituent Mn is in the trivalent state. Mn^{3+} has a d^4 electron configuration. In holosymmetric octahedral coordination, Mn^{3+} has an energetically degenerate e_g electronic state. The Jahn–Teller theorem (Jahn & Teller 1937) indicates that such an octahedron is intrinsically unstable with respect to some distorted state, and that a spontaneous distortion of the $(Mn^{3+}O_6)$ octahedron will occur. Four of the (MnO_6) octahedra [Mn(1), Mn(3), Mn(4), Mn(5)] in blatterite show four short equatorial bonds, with mean values in the range 1.90–1.94 Å, and two long apical bonds, with mean values in the range 2.27–2.30 Å; this is the typical [4 + 2]-distortion characteristic of Jahn–Teller distortion in $(Mn^{3+}O_6)$ octahedra. The Mn(2) octahedron has a [2 + 2 + 2]-distortion, with two short bonds (mean = 1.90 Å), two intermediate bonds (mean = 2.04 Å), and two long bonds (mean = 2.25 Å). Shannon *et al.* (1975) and Burns *et al.* (1994) have shown that <Mn^{3+}–O> distances in minerals are strongly affected by the degree of bond-length variation from the mean value, such that larger <Mn^{3+}–O> distances correlate with higher bond-length dispersion. The Mn(1) and Mn(3) sites have mean bond-lengths of 2.036 and 2.033 Å, respectively, which are slightly smaller than the mean bond-lengths at the other Mn sites (2.060, 2.062, 2.057 Å). These values are in accord with the occurrence of Al at these sites, as indicated by the site-scattering refinement. The mean bond-lengths are plotted against the constituent-cation radii for the octahedrally coordinated sites in blatterite (filled circles) and "Mg-blatterite" (open circles) (Fig. 1). A regression line is shown for the blatterite data, calculated for the two Sb sites, nine M sites and two of the Mn sites [Mn(1), Mn(3)]. The other three Mn sites [Mn(2), Mn(4), Mn(5)] plot slightly above the regression line. The 0.93 Fe^{3+} *apfu*, indicated by electron-microprobe data for blatterite (Table 6), is assumed to reside at one (or more) of the Mn sites: Mn^{3+} and Fe^{3+} have the same radius (0.645 Å) and the same effective scattering, and cannot be discriminated in the refinement process.

The M sites: There are nine distinct M sites with refined site-scattering values between those expected for complete occupancy by Mg and Mn, respectively. The

TABLE 5. BOND-VALENCE TABLE FOR BLATTERITE

	Sb(1)	Sb(2)	Mn(1)	Mn(2)	Mn(3)	Mn(4)	Mn(5)	M(1)	M(2)	M(3)	M(4)	M(5)	M(6)	M(7)	M(8)	M(9)	B(1)	B(2)	B(3)	B(4)	B(5)	B(6)	B(7)	B(8)	X(1)	X(2)	X(3)	X(4)	X(5)	X(6)	X(7)	Σ
O(1)				0.22																	0.98											1.95
O(2)																				0.99												1.94
O(3)							0.23												0.98								0.31					1.98
O(4)							0.25													0.99							0.21			0.10		1.84
O(5)												0.35ᵃ	0.31ᵃ									0.99										1.96
O(6)											0.30ᵃ	0.30ᵃ											0.99		0.31	0.03						1.86
O(7)										0.27					0.34ᵃ	0.28ᵃ					0.99											1.93
O(8)		0.65																				0.99		0.99								1.84
O(9)									0.33																							1.94
O(10)															0.34ᵃ	0.28ᵃ	0.99															2.20
O(11)					0.23										0.30ᵃ	0.31ᵃ		0.98										0.19	0.13			1.91
O(12)						0.22									0.34ᵃ	0.28ᵃ			0.99						0.28	0.06						1.84
O(13)																						0.99	0.99	0.99						0.05		1.89
O(14)		0.55ᵃ			0.28			0.35						0.39											0.31				0.08			1.78
O(15)		0.50ᵃ					0.61ᵃ			0.35ᵃ				0.33ᵃ					0.99													1.87
O(16)				0.33						0.34ᵃ	0.31		0.44	0.42	0.36	0.39				0.99							0.18ᵃ					2.10
O(17)										0.38									0.99						0.25ᵃ	0.07ᵃ			0.07ᵃ	0.11ᵃ		2.06
O(18)		0.83				0.22					0.51	0.32	0.43	0.32								0.96					0.29ᵃ		0.17ᵃ			1.90
O(19)			0.66ᵃ	0.86ᵃ	0.64ᵃ	0.56ᵃ	0.61ᵃ	0.35		0.34ᵃ					0.29ᵃ													0.25ᵃ	0.07ᵃ	0.11ᵃ	0.08ᵃ	0.02ᵃ	2.04
O(20)						0.63ᵃ								0.31ᵃ	0.28ᵃ	0.38																1.98
O(21)				0.46ᵃ	0.64ᵃ			0.29ᵃ				0.42	0.33		0.29ᵃ			0.99							0.28ᵃ	0.02ᵃ						1.93
O(22)															0.43	0.38		0.99														2.19
O(23)	0.63ᵃ								0.32ᵃ						0.39ᵃ	0.35ᵃ	0.99										0.29ᵃ	0.25ᵃ	0.07ᵃ		0.08ᵃ	2.04
O(24)	0.34ᵃ		0.66ᵃ		0.64ᵃ		0.61ᵃ		0.34ᵃ						0.26ᵃ	0.26ᵃ		0.99											0.17ᵃ	0.11ᵃ	0.02ᵃ	2.07
O(25)																0.38		0.99														2.01
O(26)			0.23ᵃ				0.29ᵃ																		0.26ᵃ					0.06	2.20
O(27)																												0.02	2.08
O(31)																																1.92
O(32)																																1.84
Σ	5.14	6.09	3.10	2.83	3.06	2.85	2.82	2.02	2.00	2.01	2.02	1.98	2.03	2.01	2.03	2.00	2.87	2.97	2.87	2.97	2.97	2.67	2.97	2.87	1.59	0.27	1.42	0.66	0.69	0.37	0.24	1.86

TABLE 6. CHEMICAL COMPOSITION (wt%) AND
UNIT FORMULA* (apfu) OF BLATTERITE

Sb_2O_5	12.80(24)	Sb^{5+}	3.01
TiO_2	0.19(2)		
Al_2O_3	0.33(2)	Ti^{4+}	0.09
Fe_2O_3	1.96(8)	Al	0.25
Mn_2O_3**	16.03	Fe^{3+}	0.93
B_2O_3*	14.63	Mn^{3+}	7.73
MnO	38.89(32)	Σ	9.00
MgO	14.89(9)		
Sum	99.72	Mn^{2+}	20.87
		Mg	14.06
		Σ	34.93

* calculated on the basis of 80 oxygen anions;
** calculated such that Ti^{4+} + Al + Fe^{3+} + Mn^{3+} = 9 apfu;
* calculated such that B = 16 apfu.

FIG. 1. Variation in <A–O> distances (A = Sb, M, Mn) as a function of mean radius of the constituent cations in blatterite (filled circles) and "Mg-blatterite" (open circles) of Bovin et al. (1996). The regression line for the blatterite data has the form <A–O> = 0.8325 (r) + 1.5060; r^2 = 0.999.

chemical composition determined by electron-microprobe analysis (Table 6) indicates that these sites must be occupied by Mg and Mn, and the site populations were assigned accordingly. Each of these M sites is octahedrally coordinated by six O-atoms, and the range of <M–O> distances (2.13–2.20 Å) indicates that the constituent Mn is in the divalent state. This being the case, there should be a linear relation between the <M–O> bond-lengths and the mean ionic-radius of the cations at each site. Figure 1 shows that this is the case. Final assigned site-populations are listed in Table 3.

The X sites: The X sites show extraordinary positional disorder that causes their interpretation (in terms of coordination and assignment of site populations) to be somewhat less than straightforward. Figure 2a shows the distribution of electron density in that part of the blatterite structure involving the X sites. There is a sinuous band of semi-continuous electron density snaking
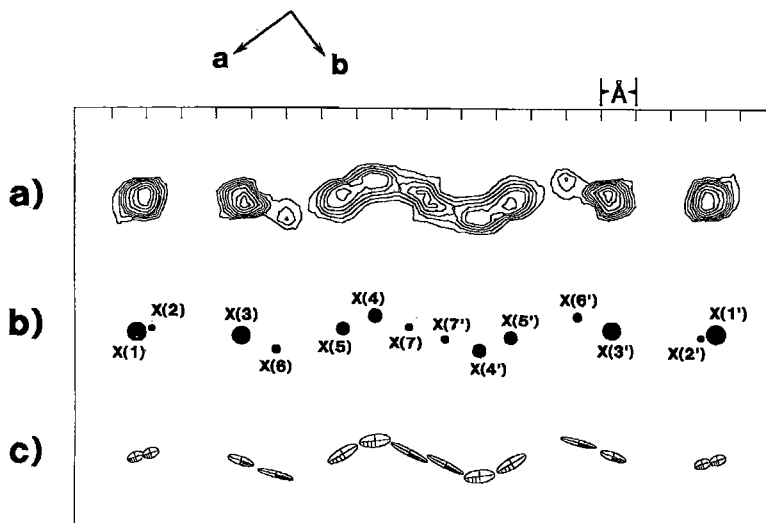
FIG. 2. Various features associated with the X sites in the structure of blatterite projected down [001]; (a) the electron density associated with the X sites calculated by difference-Fourier methods using the final structure-model with the X sites omitted; the contour interval was adjusted to provide maximum information, and is approximately 2 $e/Å^3$; (b) the X sites in the final structure-model; the size of the black circle representing each site is proportional to the amount of X-ray scattering at that site, and the X' sites are related to the X sites by a two-fold rotation the axis of which occurs between the X(7) and X(7') sites; (c) the anisotropic-displacement ellipsoids for the X sites; note how the maximum displacements follow the trend of the electron density in Figure 2a.
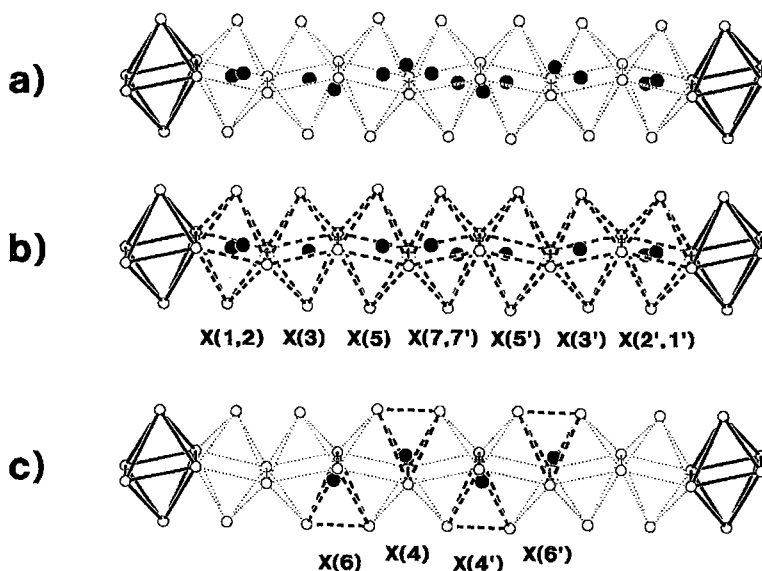
FIG. 3. Coordination around the X sites in blatterite; the X sites are shown by black circles, O atoms are shown as hollow circles, edges of octahedra defined by the array of nearest-neighbor O-atoms are shown as dotted lines, the $[M(1)O_6]$ polyhedra at each end of the chain are shown by the heavy full lines, edges of specific coordination polyhedra are shown as the heavy dashed lines. (a) All X sites and their nearest-neighbor oxygen atoms. (b) The $X(1,2,3,5,7)$ and primed-equivalent sites and their coordination octahedra. (c) The $X(4,6)$ and primed-equivalent sites and their coordination tetrahedra.

its way across the (001) plane. At each end, there are discrete atoms, but the electron density becomes increasingly smeared out toward the center of the band (Fig. 2a). Several models were tried during the course of the refinement. The model that best reproduces the electron density in this region is shown in Figure 2b, in which the sizes of the circles representing the sites are proportional to the amount of X-ray scattering at that site. Note that the X' sites are related to the corresponding X-sites by a two-fold rotation about the center of the band of electron density. Figure 2c shows the anisotropic-displacement models refined for each of the X sites. These are quite anisotropic, indicating positional disorder in addition to that represented by the array of X sites (note that the behavior of the anisotropic-displacement parameters was another factor that was used to assess the viability of the various models tried during the refinement process).

The interpretation of the coordination behavior of the X sites is somewhat tricky, and it is also apparent from the $X–X$ separations (Table 4) that certain pairs of X sites cannot be occupied simultaneously at the local scale. Figure 3a shows the X sites and the nearest-neighbor O-atoms, with the nearest O-atoms linked by dotted lines to show possible local coordinations. On the basis

of the ranges of possible $X–O$ distances and $O–X–O$ angles, two different types of coordinations were identified. The $X(1)$, $X(2)$, $X(3)$, $X(5)$ and $X(7)$ sites are octahedrally coordinated by O atoms (these coordinations are shown by the heavy broken lines in Figure 3b), whereas the $X(4)$ and $X(6)$ sites are tetrahedrally coordinated by O atoms (Fig. 3c). Details of the bond lengths of this final model are given in Table 4.

The refined site-scattering values for the X sites are given in Table 3. It is apparent from these values that the X sites are only partly occupied, and the chemical composition of blatterite (Table 6) shows that they must be occupied by Mn and $\square$ (vacancy). The $<X–O>$ distances for both octahedrally and tetrahedrally coordinated X-sites show that the constituent Mn is in the divalent state: for $X(1,2,3,5,7)$, the sum of the constituent radii is $\Sigma r = 0.83 + 1.38 = 2.21$ Å, to be compared with $<X–O>$ values of 2.22, 2.24, 2.25, 2.31 and 2.32 Å, respectively; for $X(4,6)$, $\Sigma r = 0.66 + 1.38 = 2.04$ Å, to be compared with $<X–O>$ values of 2.07 and 2.05 Å, respectively. The agreement is not exact; it is not expected to be, as we do not know the "size" of a $\square$ (vacancy) at each of these sites, but the calculated values are sufficiently close to the observed values to confirm the divalent state for the constituent Mn-atoms.

Topology of the structure

A polyhedral representation of the crystal structure of blatterite projected down [001] is shown in Figure 4. There are three principal elements apparent in this view: (1) straight chains of eleven edge-sharing octahedra extending along ~[3̄50] and ~[350], (2) zig-zag chains of octahedra extending along [3̄50] and [350], and (3) (BO₃) triangles occupying interstices between the straight and zig-zag chains (Fig. 4). Both sets of chains of octahedra share edges with similar chains displaced ~3 Å along [001] to form flat sheets and zig-zag sheets, respectively. Analogous sheets of octahedra occur in the structure of orthopinakiolite. Takéuchi *et al.* (1978) called the flat sheet the *F* wall; the zig-zag sheet was described as a *C* (corrugated) wall flanked by columns of octahedra designated as *S* columns. This notation is shown by the shading of polyhedral elements in Figure 4.

The *F* wall in blatterite is shown in Figure 5; it is terminated at each end by an *S* column of edge-sharing *M*(6) octahedra. This view of the *F* sheet shows why the different octahedra are not identified in Figure 4; the octahedra will differ, depending on the plane of the section orthogonal to [001]. The *F* wall consists of *Sb*, *Mn* and *M* octahedra. Both *Sb* octahedra and one of the *Mn* octahedra [*Mn*(2)] occur in the *F* wall, and constitute one-quarter of the constituent octahedra. Each *Sb* and *Mn* octahedron alternates with *M* octahedra to form edge-sharing chains parallel to the *c* axis, and these
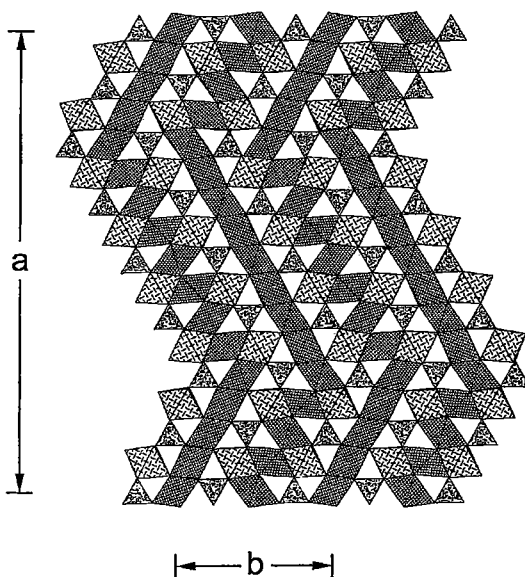
FIG. 4. Polyhedral representation of the crystal structure of blatterite viewed down [001]. Octahedra are cross-shaded (lower-density shading for *S* octahedra, higher-density shading for *F*, *C* octahedra); (BO₃) triangles are random-dot shaded.
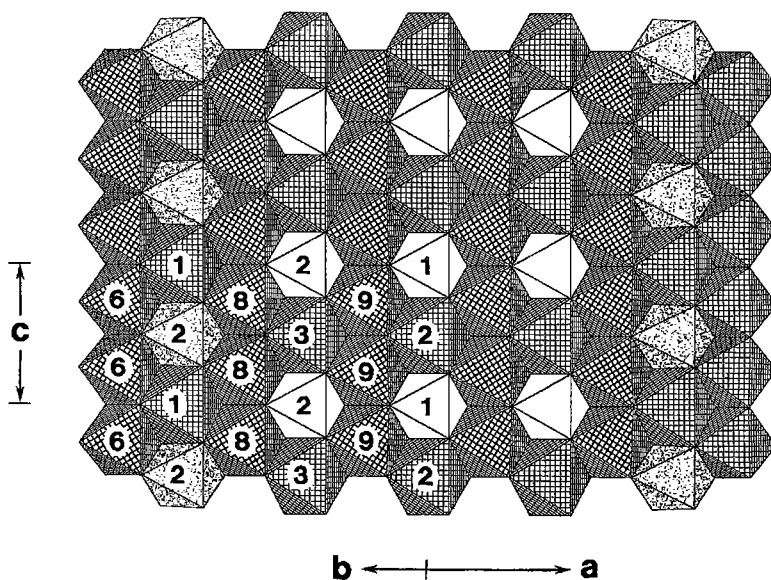
FIG. 5. The *F* wall in blatterite viewed in a direction orthogonal to the plane of the sheet; the *Sb* octahedra are unshaded, the *Mn* octahedra are shown by random-dot shading, and the *M* octahedra are shown by cross-hatched shading.
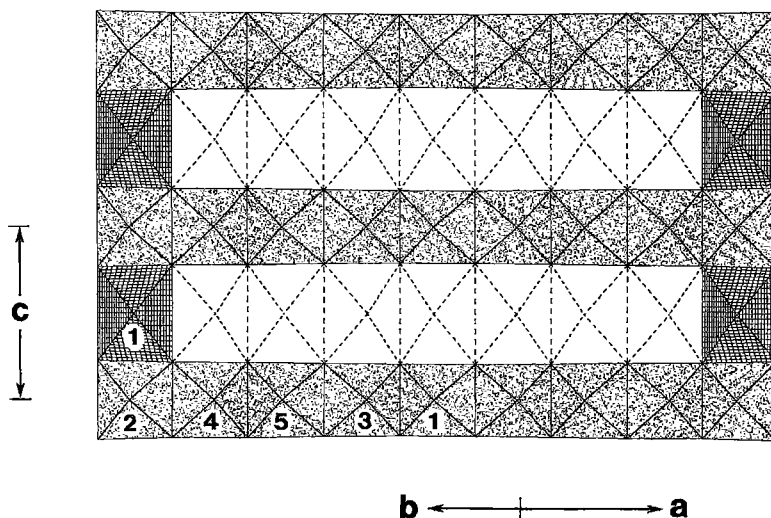
FIG. 6. The C wall in blatterite viewed in a direction orthogonal to the plane of the sheet. The legend is as in Figure 5, the X octahedra are unshaded, and their edges are denoted by dashed lines.

chains alternate with edge-sharing chains of M octahedra. In the resultant sheet (Fig. 5), the higher-charged cations (Sb^{5+} and Mn^{3+}) are never next-nearest neighbors; they are always separated from each other by at least two octahedron edge-lengths.

The C wall in blatterite (Fig. 6) consists of alternating strips of Mn and X octahedra that link in the [001] direction by sharing edges, and is terminated at each end by columns of edge-sharing Mn and M octahedra that are also part of the F walls (Fig. 5). The relative distortions of the Mn and X octahedra are very apparent in Figure 6. The shortest equatorial Mn–O distances occur in the center of the wall, and the equatorial Mn–O distances increase toward the ends of the wall [in the sequence $Mn(1,3,5,4,2)$: 1.903, 1.913, 1.936, 1.944, 1.967 Å], leading to a distinct "necking" of the strip at its center. Similarly, the chain of X octahedra increases in thickness toward the center of the wall, compensating for the adjacent strips of Mn octahedra.

The chemical formula of blatterite

We may write the structural formulae and aggregate charges of the F wall, the C wall, and the S columns of blatterite per unit cell in the following way:

F wall:	Sb_6	Mn_2	M_{24}	84^+
C wall:		Mn_{16}	M_2 X_{14}	$52^+ + X_{14}$ (1)
S column:			M_{32}	64^+
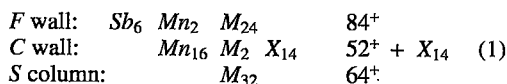
where Sb, Mn, M and X represent the different types of cation sites in blatterite. Setting $Z = 2$, this results in the formula

$$[Sb_3Mn_1M_{12}]^F [Mn_8M_1X_7]^C [M_{16}]^S (BO_3)_{16} O_{32} \quad (2).$$
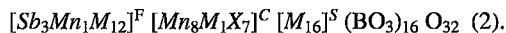
In terms of sites, we can write the *structural formula* of blatterite as

$$Sb_3 Mn_9 M_{29} X_7 (BO_3)_{16} O_{32} \quad (3).$$
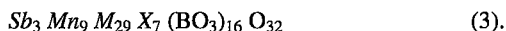
The Sb, Mn and M sites are occupied by 5^+, 3^+ and 2^+ cations, respectively, and hence the aggregate charges on each part of the blatterite structure may be written as follows: $F = 42^+$, $C = (26 + 7Z^X)^+$, $M = 32^+$. The charge on the anionic part of the structure is 112^-, and hence the total charge required of the X-site cations in the C wall is $112–42–26–32 = 12^+$. Seven X-cations can give a charge of 12^+ in the following way: 6 $M^{2+} + 1$ □ (vacancy); there are other more complex ways of achieving this charge (by incorporating M^{3+} cations and even more vacancies), but these do not seem compatible with the observed X–O distances (Table 4). Summing the cation populations of the X sites (Table 3) gives 6.0(3) Mn^{2+} *pfu*, in accord with the above calculation of the X-site content of 6.0 $M^{2+} + 1.0$ □. Arranging the content of the unit formula calculated from the electron-microprobe data gives

$$Sb_{3.01} (Mn^{3+}_{7.73}Fe^{3+}_{0.93}Al_{0.25}Ti_{0.09})_{\Sigma 9}$$
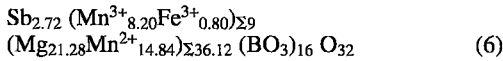$$(Mn^{2+}_{20.87}Mg_{14.06})_{\Sigma 34.93} (BO_3)_{16} O_{32} \quad (4).$$
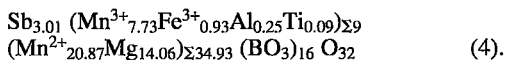
This indicates 1.07 □ at the X sites, in close agreement with the value of 1.0 □ derived from the site-scattering refinement. This formula may be generalized to

$$Sb^{5+}_3 (Mn^{3+},Fe^{3+})_9 (Mn^{2+},Mg)_{35} (BO_3)_{16} O_{32} \quad (5),$$
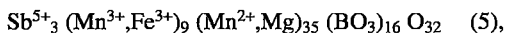
and the end-member formula for blatterite is thus Sb^{5+}_3 Mn^{3+}_9 Mn^{2+}_{35} $(BO_3)_{16}$ O_{32}.

The "blatterite mineral" of Bovin *et al.* (1996) has the formula

$$Sb_{2.72} (Mn^{3+}_{8.20}Fe^{3+}_{0.80})_{\Sigma 9}$$
$$(Mg_{21.28}Mn^{2+}_{14.84})_{\Sigma 36.12} (BO_3)_{16} O_{32} \qquad (6)$$

derived from their formula $Mg_{1.33}Mn_{1.44}Fe_{0.05}$ $Sb_{0.17}O_2(BO_3)$ when recast in the same form as blatterite given above. This formula has $Mg + Mn^{2+} = 36.12$ *apfu*, whereas the analogous sum in blatterite is 34.93 *apfu*. The above formula for "blatterite mineral" has an excess positive charge of 0.84^+ and a deficiency in Sb. Given that the Sb content of the mineral from the structure refinement is 3 *apfu*, the total excess charge on this formula is 2.24^+. This excess charge can be removed by introducing a $\square$ in the (Mg,Mn^{2+})-cation group, as is the case for blatterite, suggesting that the general formula for this mineral should be written as

$$Sb^{5+}_3 (Mn^{3+},Fe^{3+})_9 (Mg,Mn^{2+})_{35} (BO_3)_{16} O_{32} \qquad (7),$$
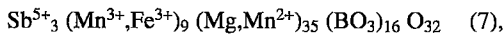
i.e., it is the Mg analogue of blatterite. The composition of the "blatterite mineral" derived from site-occupancy refinement (Bovin *et al.* 1996) has $Mg + Mn^{2+} = 36$ *apfu*; however, they *assumed* that the X sites had no vacancies, and hence effectively assumed that $Mg + Mn^{2+} = 36$ *apfu*. We suggest that blatterite and its Mg analogue have an X-site composition of $6.0\, M^{2+} + 1.0\,\square$, and that the general formula of each phase is as given above in (5) and (7), respectively.

Cation disorder at the X sites in the C walls

The chemical composition of the crystal and the $<X–O>$ bond-lengths indicate that the X cations are Mn^{2+}. In order to contribute the requisite charge, the 14 X-sites must therefore be occupied by $12\, Mn^{2+} + 2\,\square$; in accord with this requirement, the sum of the refined X-site populations is $12.0(6)\, Mn^{2+}$ per unit cell in blatterite.

Many of the X–X distances (Table 4) are not compatible with simultaneous occupancy of each site by a cation, and the disordered electron-density (Fig. 2a) is the superposition of several local (short-range) arrangements averaged over the crystal. As is apparent from Table 5, the long-range bond-valence sums at the anions coordinating the X sites are in reasonable accord with their ideal values. However, the sums must also be satisfied for each of the different *local* arrangements of cations. There are three local arrangements that are compatible with the aggregate observed electron density; these are shown in Figure 7. Note that one end of the chain of X octahedra is not related to the other end by a
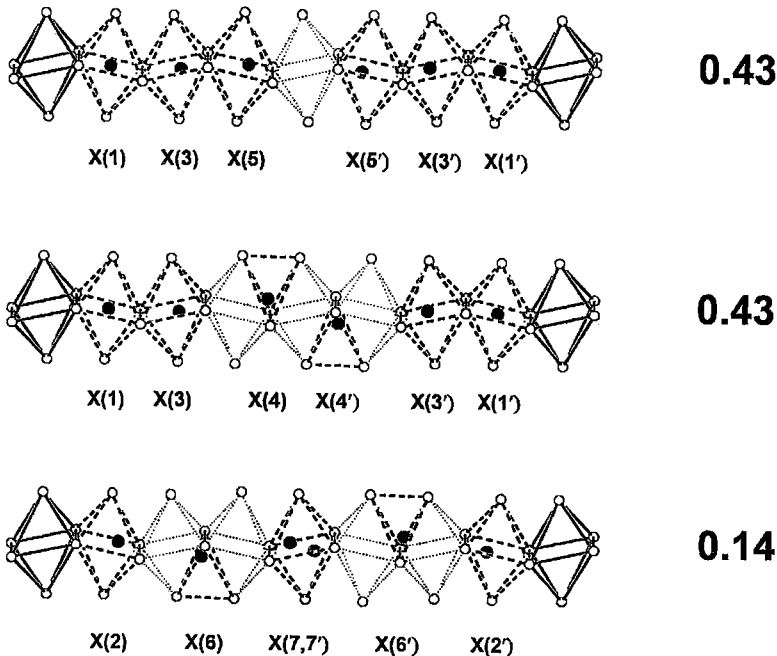

0.43

X(1)   X(3)   X(5)   X(5′)   X(3′)   X(1′)

0.43

X(1)   X(3)   X(4)   X(4′)   X(3′)   X(1′)

0.14

X(2)   X(6)   X(7,7′)   X(6′)   X(2′)

FIG. 7. Local arrangements of cations (Mn^{2+}) over the X sites in blatterite; the values to the right of each arrangement denote the frequency of the arrangement (Σfrequency = 1). Note that one end of the chain of X octahedra does not have to be related to the other end by a two-fold rotation.

two-fold rotation; crystallographic symmetry is a long-range feature of the structure, whereas the patterns of order shown in Figure 7 are short-range features. Indeed, arrangement (3) cannot occur at each end of a single chain of X octahedra, as this would result in an impossibly short $X(7)$–$X(7)$ approach of two cations (Table 4). The frequencies of the arrangements (Fig. 7) sum to agree quite closely with the refined occupancies at the X sites (Table 3). These proposed local arrangements represent the minimum unique populations that would account for the overall electron scattering, and also avoid unreasonable X–X distances.

Given the considerable positional disorder in this part of the blatterite structure, it seems surprising at first sight that there is complete *chemical* order: only Mn^{2+} occurs at the X sites, despite the large amount of Mg in the rest of the structure. The reason for this complete chemical order can be seen in Figure 6 and Table 4. The intrinsic Jahn–Teller distortion in the Mn octahedra of the C wall (Table 4) causes the Mn chains to be narrower than the S octahedra defining each end of the C wall (Fig. 6), and this broadens the chain of X octahedra. Hence the X octahedra will tend to be large owing to the inductive effects of the surrounding structure, and larger cations (*i.e.*, Mn^{2+}) will preferentially order at these sites because of this stereochemical constraint.

The next question involves the three arrangements of Figure 7: why do all three local arrangements occur? If the only requirement of the X octahedra were that they should incorporate a vacancy (*i.e.*, $X_7 = Mn^{2+}_6 + \square$), any one of the arrangements in Figure 7 would suffice. In this regard, there are two possibilities: (1) the occurrence of all three arrangements is driven by the accompanying stabilization due to increase in entropy; (2) each arrangement is induced by the local stereochemistry. Possibility (1) does not seem reasonable, as a much higher entropy-driven stabilization could occur by randomly disordering 6 Mn^{2+} + 1 $\square$ over the seven X-octahedra, whereas the observed electron-density (Fig. 2a) shows that this possibility does not occur. Hence we may deduce that the occurrence of the three arrangements of short-range order must be related to the local stereochemistry. The X octahedra are intimately associated with the columns of S octahedra (Fig. 4). The S octahedra are occupied by Mn^{2+} and Mg, and it is possible that the local arrangements of the X cations are related to the occupancy of the locally associated S-octahedra. The mean composition of the S octahedra in the blatterite examined here is $0.57\ Mn^{2+} + 0.43$ Mg, and there are four independent S octahedra [$M(4)$, $M(5)$, $M(6)$, $M(7)$]. If the local arrangements (1) Mn^{2+}–Mg–Mn^{2+}–Mg, (2) Mg–Mn^{2+}–Mg–Mn^{2+} and (3) Mn^{2+}–Mn^{2+}–Mn^{2+} occur with the same frequencies as the local arrangements of X cations in Figure 7 (0.43, 0.43, 0.14), the long-range composition of the S sites would be $0.57\ Mn^{2+}$ and 0.43 Mg, suggesting the possibility of a spatial association between cation ordering at the X and S sites.

THE CRYSTAL CHEMISTRY OF THE Mn^{3+}-BEARING ZIGZAG BORATES

Takéuchi *et al.* (1978) and Takéuchi (1978, 1997) introduced the idea of F walls, C walls and S columns to describe the structure of orthopinakiolite and its relation to the structure of pinakiolite. This description works very well for the structures of several other (commonly paragenetically) related borate minerals; these are listed in Table 7. In order to facilitate comparison of these structures, we have changed the site nomenclatures used in previous studies of other structures to make them conformable with the systematic site-nomenclature used here for blatterite; details are given in Table 8. We call these Mn^{3+}-bearing minerals the *zigzag borates* owing to the striking zigzag patterns that are apparent when these structures are viewed down their $3n$ Å axis (*e.g.*, Fig. 4); our discussion focuses primarily on those structures for which $n = 2$.

Structural relations

The structures of these minerals are shown in Figure 8, in which the shadings denote the F wall, the C wall and the S columns. Each F wall is terminated at each end by an S column. The ends of each C wall meld with adjoining F walls such that the terminal octahedra of each F wall also belong to the attached C-wall (this is why, in Table 8, some octahedra in each structure are identified as belonging to both the F wall and the C wall). Note that, for pinakiolite, the F and C walls do not merge. There are equal numbers of octahedra in the F wall, the C wall and the S column, and hence we can write each structure as $F_nC_nS_n$, where n is the number of octahedra in each structural component. (Note that when considering the stoichiometries of such structures, it is important to remember that the terminal octahedra of the F wall and the C wall are common to each unit, and should not be counted twice.) Although ludwigite (*Pbam*) is normally considered as the type structure of this group of isostructural minerals, here we refer to fredrikssonite, as it is compositionally similar to the other (*Pnnm*) Mn^{3+}-bearing zigzag borates. For fredrikssonite, $n = 3$ (although fredrikssonite is a 3 Å structure), for orthopinakiolite, $n = 5$, for takéuchiite, $n = 7$, and for blatterite, $n = 9$. The next (un-named) member of this series has $n = 11$; details of the unit cell are given in Table 7. Pinakiolite (*C2/m*) (Fig. 8f) is the end-member of this series: $F_\infty C_\infty S_\infty$.

In all of these structures, the direction of the wall is changed [in the (001) plane] by a glide operation orthogonal to [100]. If $c \approx 3$ Å (as in fredrikssonite), this operation is a b glide; if $c \approx 6$ Å (as in orthopinakiolite, takéuchiite and blatterite, Table 7), this operation is an n glide. The type of glide plane is related to the chemical composition and stereochemistry of the F wall. Fredrikssonite and pinakiolite have chemically and structurally simple F-walls (Table 8, Figs. 9a, f),

TABLE 7. THE ZIGZAG BORATES

Mineral	Formula	a (Å)	b (Å)	c (Å)	Sp. Gr.	Structure	Ref.	V_{rel}*	Oct.**	$(BO_3)^†$
			3 Å Zigzag Borates							
Azoproite	$Mg_2(Fe^{3+},Ti^{4+},Mg)(BO_3)O_2$	9.26(1)	12.25(1)	3.01(1)	Pbam	$F_3C_3S_3$	1	1	12	4
Bonaccordite	$Ni_2Fe^{3+}(BO_3)O_2$	9.213(6)	12.229(7)	3.001(2)	Pbam	$F_3C_3S_3$	2	1	12	4
Fredrikssonite	$Mg_2Mn^{3+}(BO_3)O_2$	9.198(2)	12.528(3)	2.965(1)	Pbam	$F_3C_3S_3$	[3]	1	12	4
Ludwigite	$Mg_2Fe^{3+}(BO_3)O_2$	9.257(1)	12.282(1)	3.0234(2)	Pbam	$F_3C_3S_3$	[4]	1	12	4
Vonsenite	$Fe_2^{2+}Fe^{3+}(BO_3)O_2$	9.463(1)	12.305(1)	3.073(1)	Pbam	$F_3C_3S_3$	[5]	1	12	4
Hulsite	$(Fe^{2+},Mg)_2(Fe^{3+},Sn)(BO_3)O_2$	10.695(4)	3.102(1)	5.431(1)	P2/m		[6]	–	–	–
Magnesiohulsite	$(Mg,Fe^{2+})_2(Fe^{3+},Sn^{4+},Mg)(BO_3)O_2$	–	–	–	–		(7)	–	–	–
			6 Å Zigzag Borates							
Chestermanite*	$Mg_2(Fe^{3+},Mg,Al,Sb^{5+})(BO_3)O_2$	18.535(3)	12.273(1)	6.043(1)	Pnnm	$F_5C_5S_5$	[8]	4	48	16
Orthopinakiolite*	$(Mg,Mn^{2+})_2Mn^{3+}(BO_3)O_2$	18.357(4)	12.591(2)	6.068(1)	Pnnm	$F_5C_5S_5$	[9]	4	48	16
Takéuchiite*	$(Mg,Mn^{2+})_2(Mn^{3+},Fe^{3+})(BO_3)O_2$	27.585(4)	12.561(3)	6.027(2)	Pnnm	$F_7C_7S_7$	[10]	6	72	24
Blatterite	$Sb_3^{5+}(Mn^{3+},Fe^{3+})_9(Mn^{2+},Mg)_{35}(BO_3)_{16}O_{32}$	37.654(8)	12.615(3)	6.2472(8)	Pnnm	$F_9C_9S_9$	[11]	8	96	32
"Mg-Blatterite"	$Sb_3^{5+}(Mn^{3+},Fe^{3+})_9(Mg,Mn^{2+})_{35}(BO_3)_{16}O_{32}$	37.384(11)	12.568(3)	6.200(2)	Pnnm	$F_9C_9S_9$	[12]	8	96	32
$F_{11}C_{11}S_{11}$	–	46.3	12.52	6.12	Pnnm	$F_{11}C_{11}S_{11}$	–	10	120	40
Pinakiolite*·**	$(Mg,Mn^{2+})_2(Mn^{3+},Sb^{3+})(BO_3)O_2$	21.79(1)	5.977(5)	5.341(5)	C2/m	$F_∞C_∞S_∞$	[13]	–	–	–

* Formulae as given in Fleischer & Mandarino (1995); see text for new formulae. ** $\beta = 95.83(5)°$; * V_{rel}: relative cell-volume ~ $V/V_{ludwigite}$; ** Oct: number of octahedra in unit cell; † (BO_3): number of (BO_3) groups in unit cell
References: [ ] denotes crystal-structure work: (1) Konev *et al.* (1970); (2) DeWaal *et al.* (1974); [3] Burns *et al.* (1994); [4] Bonazzi & Menchetti (1989); [5] Swinnea & Steinfink (1983); [6] Konnert *et al.* (1976); [7] Yang *et al.* (1985); [8] Alfredsson *et al.* (1991); [9] Takéuchi *et al.* (1978); [10] Norrestam & Bovin (1987); [11] this study; [12] Bovin *et al.* (1996), modified in this study; [13] Moore & Araki (1974).

compatible with a c repeat of only 3 Å (*i.e.*, one octahedron along the c axis). The other zigzag borates have chemically (and structurally) more complicated F-walls (Table 8), and hence require a longer repeat-distance in the c direction to incorporate these more complicated chemical compositions. An n glide gives double the repeat distance for the F wall in the c direction which, when combined with the increase in the a dimension, gives sufficient room for the F wall to incorporate the required combination of different types of cation sites (Fig. 9).

The F walls

We can consider the F walls (Fig. 9) to be constructed from four types of chains of edge-sharing octahedra of the form $[M\phi_4]$ extending along the $3n$ Å direction: A: M ($= Mn^{2+}$,Mg) octahedra; B: Mn ($= Mn^{3+}$) octahedra; C: alternating M and Mn octahedra; D: alternating M and Sb ($= Sb^{5+}$) octahedra. Fredrikssonite has the sequence (BAB); orthopinakiolite has the sequence $(CABAC)$; takéuchiite has the sequence $(CABABAC)$; blatterite has the sequence $(CADADADAC)$; pinakiolite has the sequence $(AB)^*$ (where * denotes an infinitely repeating sequence). These sequence variations are driven by the local bond-valence requirements of the O atoms of the F walls. Details of the anion coordina-

tions in blatterite as compared to orthopinakiolite and takéuchiite are shown in Figure 10 and Table 9. There are two types of anion coordination in orthopinakiolite and takéuchiite: coordination by B, Mn^{3+} and 2 Mg (Figs. 10a, 9c, 9d) and coordination by 2 Mn^{3+} and 2 Mg (Figs. 10c, 9c, 9d). The Pauling bond-strengths, which are shown in Figure 10a and Table 9, are greater ($2^1/_6$) and less ($1^2/_3$ vu) than the ideal value of 2.0 vu, allowing bond-length relaxation within the F wall to compensate for these deviations from the valence-sum rule (Brown 1981, Hawthorne 1994). The incorporation of the high-valence cation Sb^{5+} into the F wall in blatterite is most easily accomplished by having Sb^{5+} coordinated to anions analogous to those anions in orthopinakiolite and takéuchiite that have the lowest Pauling bond-strength sums [*cf.* Hawthorne (1978) for the analogous case in amphiboles]. Thus Sb^{5+} replaces Mn^{3+} in arrangement (c) (Fig. 10) to produce arrangement (d), with a bond-strength sum of $1^5/_6$ vu. However, there are insufficient anions with this type of coordination to completely coordinate Sb^{5+} in blatterite, and hence type-(a) anions (Fig. 10) must be involved as well. Again, Sb^{5+} replaces Mn^{3+} (Figs. 10a, b), producing a high bond-strength sum ($2^1/_2$ vu) around the anions. To help compensate for this high sum and allow some local bond-length relaxation, remaining type-(a) atoms not linked to Sb^{5+} also change their coordination,

(a) Fredrikssonite
(b)

(c) Orthopinakiolite

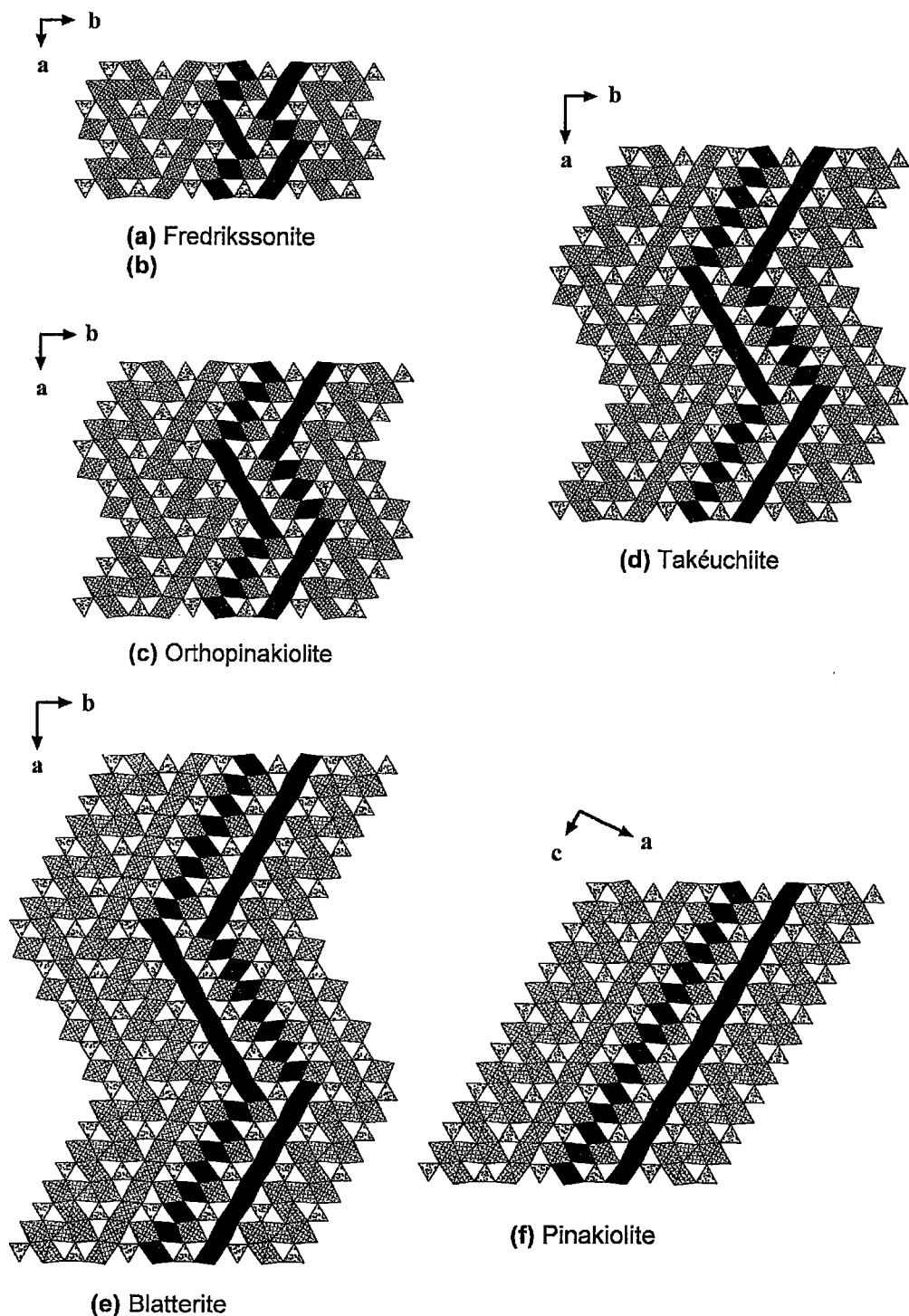**(d)** Takéuchiite

(e) Blatterite

(f) Pinakiolite

FIG. 8. Polyhedral representations of the Mn^{3+} zigzag borates viewed down [001] ([010] for pinakiolite): (a) fredrikssonite (ludwigite-type), (b) hypothetical *Pnnm* $F_3C_3S_3$ structure, (c) orthopinakiolite, (d) takéuchiite, (e) blatterite, and (f) pinakiolite. The legend is as in Figure 4; a neighboring pair of *F* and *C* walls have been shaded black.

TABLE 8. RELABELING OF SITES AND THEIR ROLE IN THE UNITS OF THE Mn³⁺-BEARING ZIGZAG BORATE STRUCTURES

Site	Multiplicity	Type*	Unit**	Site	Multiplicity	Type	Unit
FREDRIKSSONITE				**TAKÉUCHIITE**			
M(1)	2	M	F	M(1)	4	M	F
M(2)	2	M	C	M(2)	2	X	C
M(3)	4	M	S	M(3)	2	Mn	C
M(4)	4	Mn	F,C	M(4)	8	M	S
				M(5)	8	M	S
ORTHOPINAKIOLITE				M(6)	8	M	S
				M(7)	4	X	C
M(1)	2	Mn	F	M(8)	4	Mn	C
M(2)	2	Mn	F	M(9)	4	X	C
M(3)	2	Mn	C	M(10)	4	Mn	C
M(4)	2	X	C	M(11)	4	M	F,C
M(5)	8	M	S	M(12)	4	Mn	F,C
M(6)	4	Mn	C	M(13)	8	M	F
M(7)	4	X	C	M(14)	4	Mn	F
M(8)	4	Mn	F,C	M(15)	4	Mn	F
M(9)	4	M	F,C				
M(10)	8	M	S	**PINAKIOLITE**			
M(11)	8	M	F				
				Mn(1)	2	Mn	C
				Mn(2)	2	Mn	C
				Mn(3)	4	Mn	F
				Mg(1)	2	X	C
				Mg(2)	2	X	C
				Mg(3)	4	M	F
				Mg(4)	8	M	S

* Labelled according to the current nomenclature for blatterite: Mn is occupied by Mn³⁺, M is occupied by (Mn²⁺,Mg), X are the disordered sites of the C wall occupied by Mn²⁺, Mg, □. Minor Fe³⁺ may be assigned to Mn, M and X sites.
** Indicates the structural element to which the site belongs: F = F wall; C = C wall; S = S column.

replacing Mn^{3+} by Mg or Mn^{2+} and reducing the bond-strength sum to 2 vu. There are twice as many type-(d) anions as there are type-(b: 2½ vu) anions, and thus type-(d) anions can cooperatively relax with type-(b: 2½ vu) anions to help compensate for bond-strength anomalies to both types of anions. It is also apparent from Figure 10 that octahedra occupied by Sb^{5+} cannot share edges, as this would produce unreasonably large bond-strength sums at anions common to both Sb-octahedra. Chains of alternating Sb^{5+} and Mg or Mn^{2+} octahedra may then replace chains of Mn^{3+} octahedra with preservation of the Pauling bond-strengths to the oxygen

atoms of the F-wall. However, for every n Mn^{3+} chains replaced by (Sb^{5+} + Mg or Mn^{2+}), there is a net surplus cation-charge of $(2n)^+$ per unit cell. As a result, cation sites outside the F-wall must be involved in helping maintain overall electroneutrality.

The C walls

One of the most curious features of each of the Mn^{3+} members of this group is the pattern of disordered cation-sites within the C-wall. If this feature is attributed to Jahn–Teller distortion of neighboring Mn^{3+} octahedra, the following questions are pertinent: 1) If Mn^{3+} is responsible, and the associated Jahn–Teller distortion drives the neighboring positional disorder, what are the details of the mechanism? 2) Some investigators have assigned vacancies to the disordered regions [pinakiolite: Moore & Araki (1974); orthopinakiolite; Takéuchi et al. (1978); blatterite: this work] and others have not [takéuchiite: Norrestam & Bovin (1987); "Mg-blatterite": Bovin et al. (1996)]. What role do vacancies play in these structures? 3) Fredrikssonite contains significant Mn^{3+}; why is there no associated positional disorder? 4) Within the F walls of orthopinakiolite and takéuchiite are chains of edge-sharing [4 + 2]-distorted Mn^{3+} octahedra; why is there no associated positional disorder of the neighboring cations in these F walls? 5) Orthopinakiolite, takéuchiite and blatterite are all 6 Å Mn^{3+} borates that have Pnnm symmetry and show simple expansions of their C walls, from 5 → 7 → 9 octahedra, respectively (Figs. 11c, d, e). Associated progressive lengthening of the F walls (Figs. 9c, d, e) and increase in the number of S columns (Figs. 8c, d, e) also occur. It becomes immediately apparent that the simplest structural member of this series should have a C wall (and F wall) that is three octahedra wide; this hypothetical structure is shown in Figures 8b, 9b, 11b. Is there a structural explanation why this simple derivative structure has not yet been reported?

The outer C-wall columns: Columns of edge-sharing octahedra define the outer margins of the C walls (Fig. 11), in which Mn octahedra alternate with M octahedra. Distortion in the equatorial plane of these octahedra causes a relative widening of the Mn

TABLE 9. COMPARISON OF ANION COORDINATIONS AND BOND-VALENCE (vu) ARRANGEMENTS IN THE F WALLS OF ORTHOPINAKIOLITE, TAKÉUCHIITE AND BLATTERITE

Figure	Mineral	O atoms	Coordination and bond-valence arrangement
10(a)	orthopinakiolite takéuchiite	O(15), O(16) O(9), O(10), O(17), O(18)	$1/6(Mg^{2+}) + 1/6(Mg^{2+}) + 1/3(B^{3+}) + 1/6(Mn^{3+}) = 2\ 1/6$
10(b)	blatterite blatterite	O(10), O(23), O(28) O(9), O(22), O(27)	$1/6(Mg^{2+}) + 1/6(Mg^{2+}) + 1/3(B^{3+}) + 1/6(Sb^{5+}) = 2\ 1/2$ $1/6(Mg^{2+}) + 1/6(Mg^{2+}) + 1/3(B^{3+}) + 1/6(Mg/Mn^{2+}) = 2$
10(c)	orthopinakiolite takéuchiite	O(1) O(1), O(2)	$1/6(Mn^{3+}) + 1/6(Mn^{3+}) + 1/6(Mg^{2+}) + 1/6(Mg^{2+}) = 1\ 2/3$
10(d)	blatterite	O(17), O(18), O(29)	$1/6(Sb^{5+}) + 1/6(Mg/Mn^{2+}) + 1/6(Mg/Mn^{2+}) + 1/6(Mg^{2+}) = 1\ 5/6$

(a) Fredrikssonite   (b)   (c) Orthopinakiolite   (d) Takéuchiite

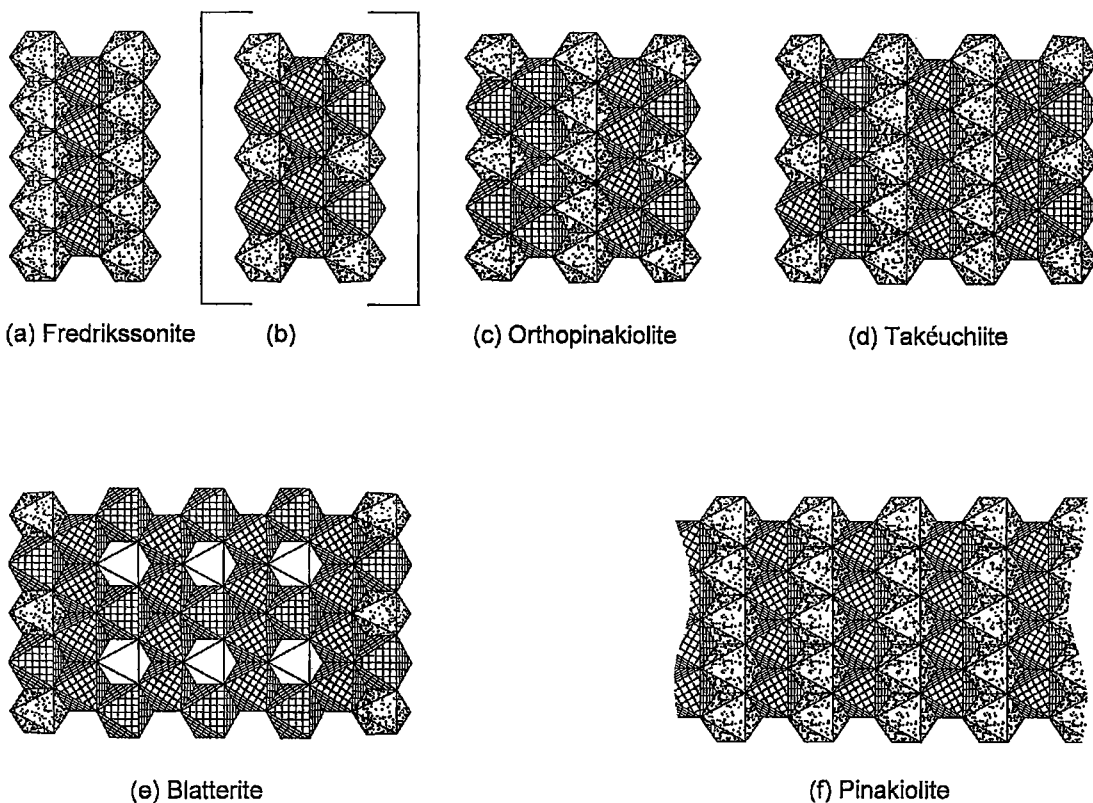(e) Blatterite   (f) Pinakiolite

FIG. 9. The F walls in (a) fredrikssonite, (b) hypothetical $Pnnm$ $F_3C_3S_3$ structure, (c) orthopinakiolite, (d) takéuchiite, (e) blatterite, and (f) pinakiolite. The legend is as in Figures 5 and 6.

octahedra toward the outer edge, coupled to a complementary contraction in the M octahedra. These Mn sites form short Mn–O bonds (1.905 Å: Fig. 11c; 1.918 Å: Fig. 11d, 1.895 Å: Fig. 11e) with the equatorial O-atoms along the outermost edge, intermediate Mn–O bonds (1.963 Å: Fig. 11c, 1.979: Fig. 11d, 2.039 Å: Fig. 11e) with the equatorial O-atoms on the inner side of the columns of octahedra, and long Mn–O bonds (2.192, 2.349 Å: Fig. 11c; 2.138, 2.227 Å: Fig. 11d; 2.165, 2.326 Å: Fig. 11e) to the apical O-atoms. This conforms to [(2 + 2) + 2]-coordination of these Mn octahedra that facilitates attachment of this column of octahedra to the outermost M column of octahedra in the F wall (Figs. 8, 9, 11).

The inner C wall: Inside the outermost columns of the C walls, strips of positionally disordered cations alternate with strips of [4 + 2]-distorted Mn octahedra (Figs. 11b–f). Within a given column through the central region of the C wall, all short Mn–O equatorial bonds lie (approximately) in a common plane. This alignment of Mn–O bond-shortening results in a relative contraction of the strips of Mn octahedra and com-

plementary expansion of the intervening strip of octahedra (Figs. 11b–f). The bonding environment of the unique part of this extended octahedral strip is shown in Figure 12, where the $X*$ cation-sites have been constrained to occupy ordered central positions of the octahedra. Bond valences (*vu*) for each bond (calculated for X-site occupancy by Mn^{2+}) are shown, as well as the resulting valence-sums (circled) at the coordinating O-atoms and $X*$ cation-sites. There is a progressive decrease in bond-valence sums (incident at the cations) toward the center of the octahedral strip, in the sequence $M(1)* \rightarrow X(7)*$, whereas the sums at the equatorial O-atoms increase from ~2.00 to 2.14 *vu*. This mismatch of valence sums, especially in the center of the strip [$X(5)*$–$X(7)*$–$X(5')*$], clearly shows that centrally positioned Mn^{2+} cations cannot meet the necessary bonding requirements of this region of the structure.

Next, the relative flexibility of the coordinating O-atoms can be examined in terms of their ability to relax their positions according to the bonding requirements of central $X*$ sites. The equatorial O-atoms form two strong bonds (~0.63 *vu*) to a pair of Mn^{3+} cations
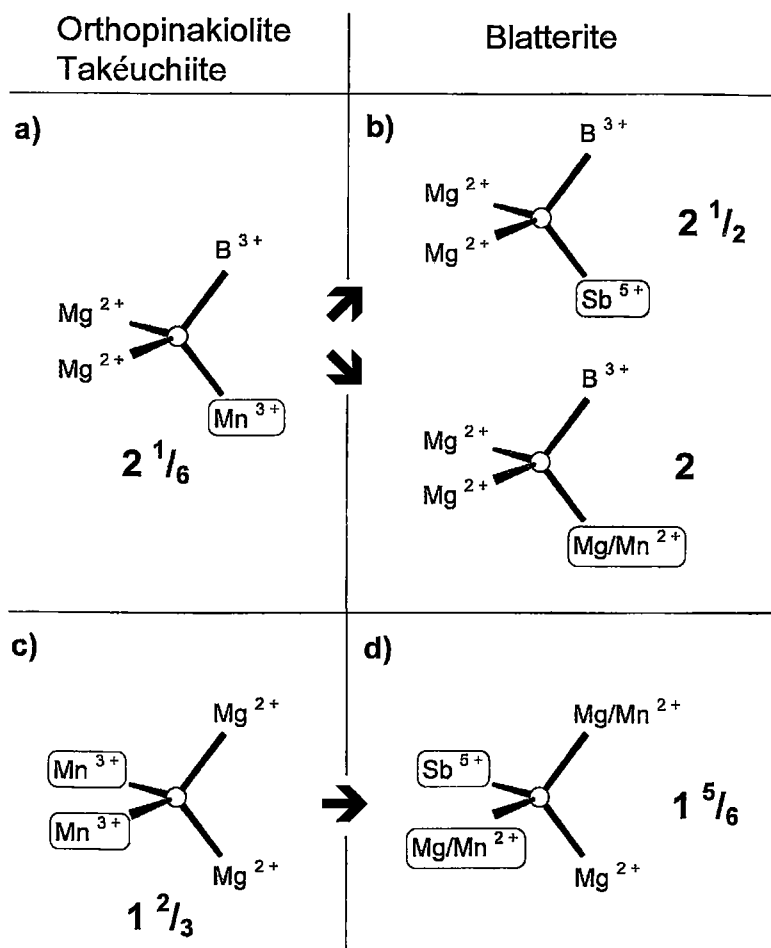
FIG. 10. Details of the anion coordination in the F walls of (a), (c) orthopinakiolite and takéuchiite, and (b), (d) blatterite; details of the anion identity for each structure are given in Table 9.

(Table 5), and this bond configuration is symmetrically related across the (001) mirror planes at $z = 0$, ½. Attempts to reposition these O-atoms to satisfy the bonding requirements of the X sites disrupts the [4 + 2]-geometry of the Mn^{3+} octahedra. Adjacent pairs of apical O-atoms share two vertices with (BO_3) triangles (Fig. 8). These bridging (BO_3) groups are very constraining from a geometrical viewpoint, as only very minor rotations of these groups may occur. The Jahn–Teller-driven [4 + 2]-distortion of the Mn octahedra, in combination with an architecture involving rigid (BO_3) triangles, significantly constrains the O-atom positions. The X cations in this region are subject to this constrained anion environment and will try to adjust their positions in order to satisfy the remaining bond-valence requirements of these O-atoms. In doing so, these X

cations must also fulfill their own bond-valence requirements, which is not possible from centrally located sites (Fig. 12). Therefore, the X cations must spontaneously move off-center. Attempts to order "off-center" X sites (consistent with $Pnnm$ symmetry) that are fully occupied quickly introduces two problems: (1) equatorial O-atoms become severely overbonded, and (2) unreasonable Mn^{2+}–Mn^{2+} distances ensue. Resolution of these problems occurs when: (1) vacancies are introduced at the X sites, in combination with (2) more than one local arrangement of X-cations, and (3) $Mn^{2+} \leftrightarrow Mg$ substitution in the adjoining S-column octahedra (Fig. 8) coupled with changing bond-valence requirements of the adjacent O-atoms.

Structure (b): This hypothetical structure was constructed by progressive condensation of these
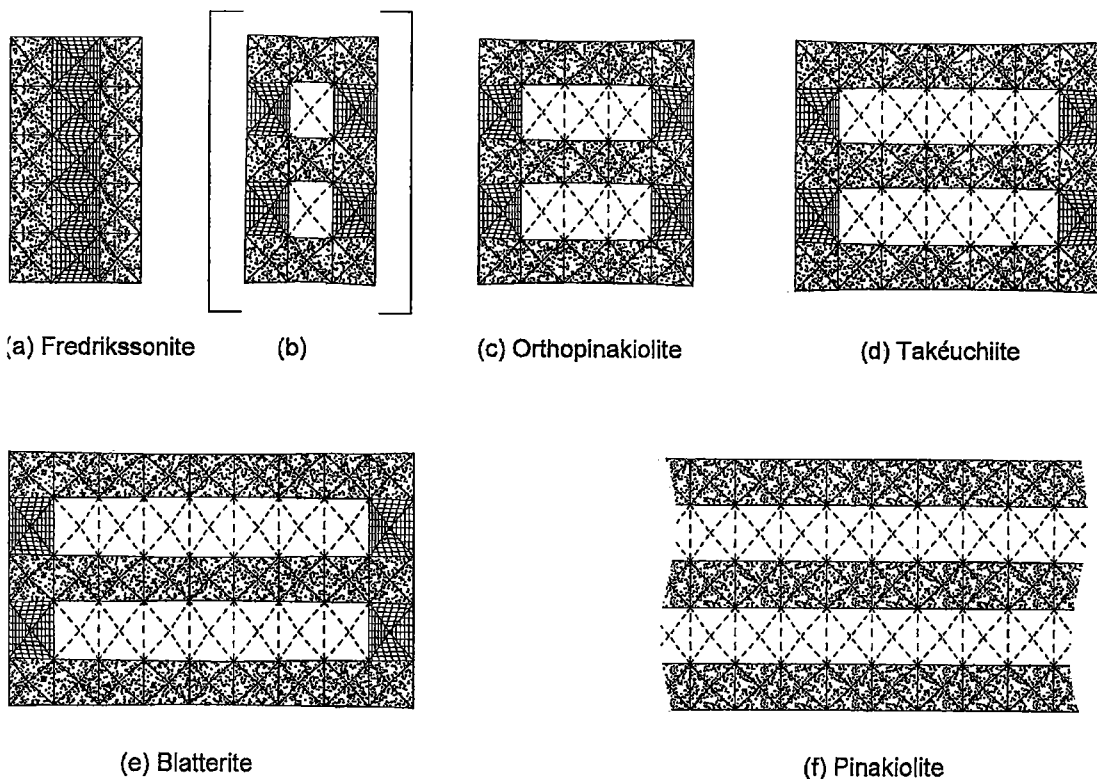
(a) Fredrikssonite   (b)   (c) Orthopinakiolite   (d) Takéuchiite

(e) Blatterite   (f) Pinakiolite

FIG. 11. The C walls in (a) fredrikssonite, (b) hypothetical $Pnnm$ $F_3C_3S_3$ structure, (c) orthopinakiolite, (d) takéuchiite, (e) blatterite, and (f) pinakiolite. The legend is as in Figures 5 and 6.

structures in the sequence blatterite $\rightarrow$ takéuchiite $\rightarrow$ orthopinakiolite $\rightarrow$ (b) (Figs. 8, 9, 11). By analogy with takéuchiite and orthopinakiolite, this hypothetical Sb-free species has cell dimensions $a \approx 9.1$, $b \approx 12.6$, $c \approx 6.1$ Å and space-group symmetry $Pnnm$. It is interesting to note that this structure would be the simplest member of this group, and that it has never been reported as a mineral or a synthetic phase. The answer lies in the nature of the C walls as described in the preceding section: the C wall (Fig. 11b) contains a single central column in which the [4 + 2]-distorted Mn octahedra would be above and below the intervening octahedron. This intervening octahedron would be inhospitable to occupancy by a centrally located X cation (*cf.* blatterite, Figs. 11, 12). Movement of this X cation off-center does not resolve the situation, as this produces cation–cation interferences with the M cations in the end columns; necessary positional disorder is inhibited, and this structure is therefore not expected to form.

Fredrikssonite: Fredrikssonite has a structure (*Pbam*) different from that of the other Mn^{3+} members of this group (Figs. 8, 9, 11), and is the only member that does not show the characteristic positional disorder of cations (Burns *et al.* 1994). The C wall (Fig. 11a)

contains end columns of edge-sharing Mn octahedra that flank a single column of M octahedra. The Mn octahedra are not [4 + 2]-distorted; instead, they have an unusual [(2 + 2) + 2]-coordination that is a result of local bond-valence requirements (Burns *et al.* 1994). The [(2+ 2) + 2]- coordination of the Mn octahedra does not create an inhospitable neighboring environment, and there is no positional disorder of the adjacent M cations.

F wall in takéuchiite: The three central columns of octahedra of the F wall in takéuchiite are comprised of outer [4 + 2]-distorted Mn octahedral columns, with an intervening column of M octahedra (Fig. 9d). In this configuration, the neighboring [4 + 2]-distortions do not line up with each other; the short equatorial Mn–O bonds from one column of Mn octahedra lie within a plane that is staggered from the plane containing the short Mn–O equatorial bonds of the other column of Mn octahedra (Figs. 8d, 9d). As a result, M cations are able to occupy ordered sites between these neighboring columns of Mn octahedra.

For orthopinakiolite, takéuchiite, blatterite and pinakioite (and their isostructural analogues), we have assumed that the disorder of the X-site cations is static; there also could be dynamic disorder, as has been ob-
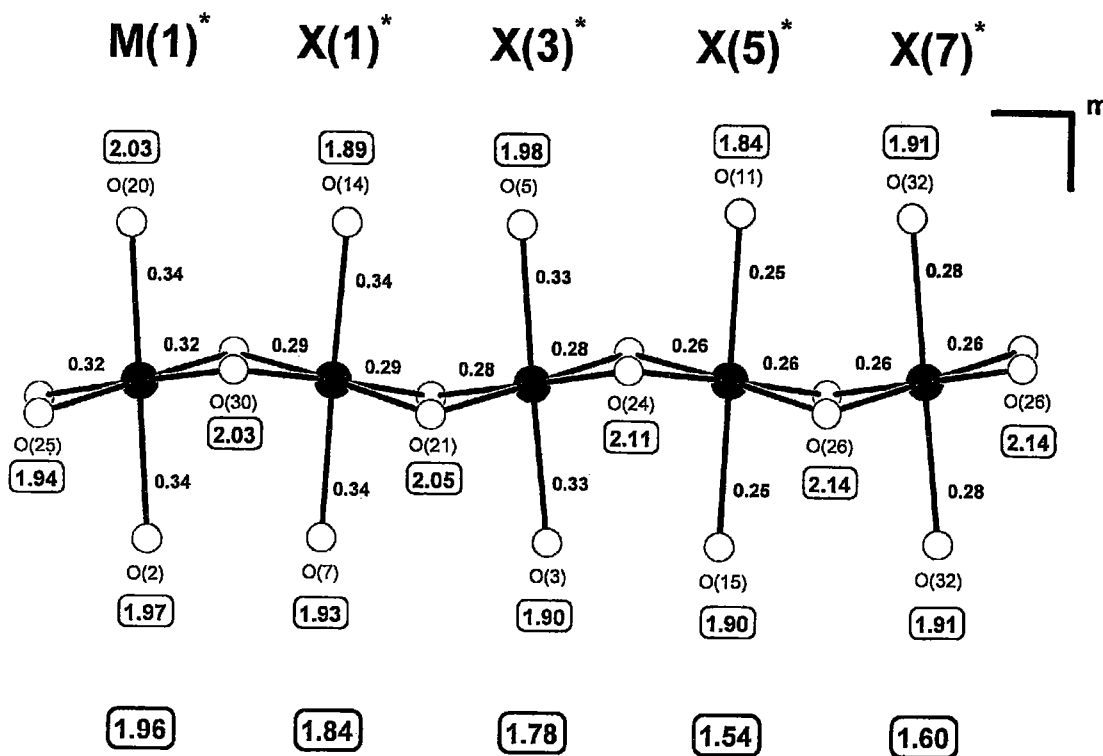
FIG. 12. Details of the Pauling bond-strengths (valence units) associated with centrally located (X^*) Mn^{2+} cations along the octahedral strip in the C-wall of blatterite.

served in some ionic conductors. However, this latter possibility is unlikely, as we show later that the details of the disorder may be coupled to the constitution of the locally associated octahedra of the S columns. Superposition of a variety of local arrangements in these minerals (e.g., as suggested for blatterite in Fig. 7) will produce the unusual distributions of electron density observed.

CHEMICAL FORMULAE

For blatterite, we have proposed that there are three local arrangements of Mn^{2+} cations that involve two vacancies per unit cell (Table 3, Fig. 7). If one compares the pattern of electron-density distribution in the disordered region of blatterite (Figs. 2, 3) and takéuchiite (Norrestam & Bovin 1987; Fig. 8), the resemblance is striking. This similarity, in combination with the fact that the C walls are simple derivatives of each other (Fig. 11), suggests that the two minerals share common attributes in this region of the structure (even though the F walls differ). If the large isotropic-displacement parameter associated with the central X-cation [at the $M(4)$ site] in orthopinakiolite (Takéuchi et al. 1978) is interpreted as representing two disordered sites, then ortho-

pinakiolite can also be described as containing the same disordered pattern.

In Table 10, structural features of the F wall, S column and C wall of orthopinakiolite, takéuchiite, blatterite and other possible derivative structures are presented. They are all 6 Å $Pnnm$ structures that contain Mn^{3+} and have the same C-wall architecture. These minerals differ in the makeup of their F walls: structures containing Mn columns are designated as B structures, and those containing columns of $-Sb-M-Sb-M-$ octahedra are designated as D structures; the integer N is defined as the number of such columns in the F wall (cf. Fig. 9), and the structures are labeled by the symbols $B(N)$ and $D(N)$ (Table 10).

This division into B and D structures is an important one, as it focuses on the different mechanisms used for attaining electroneutrality in these structures.

The D structures

Table 10 gives the site content of each of the walls of each structural component. The structural formula of any mineral may thus be written by summing the sites in the F and C walls and S column, and dividing the numbers of sites by 2 (as $Z = 2$ for all these structures).

TABLE 10. SITE COMPOSITIONS FOR THE Mn^{3+} (Pnnm) DERIVATIVE STRUCTURES

F-Type[1]	Mineral	Oct.[3]	F-wall[4]		S-column[4]		C-wall[4]		F+S+C	$[BO_3O_2]^{?-}_y$
B(0)[2]	Figs. 8b,9b,11b	24	Mn_2M_6	(18⁺)	M_8	(16⁺)	$Mn_4M_2X_2$	(20⁺)	54⁺	56⁻ (Y=8)
B(1)	orthopinaklolite	48	Mn_6M_{10}	(38⁺)	M_{16}	(32⁺)	$Mn_8M_2X_6$	(40⁺)	110⁺	112⁻ (Y=16)
B(2)	takéuchiite	72	$Mn_{10}M_{14}$	(58⁺)	M_{24}	(48⁺)	$Mn_{12}M_2X_{10}$	(60⁺)	166⁺	168⁻ (Y=24)
B(3)	—	96	$Mn_{14}M_{18}$	(78⁺)	M_{32}	(64⁺)	$Mn_{16}M_2X_{14}$	(80⁺)	222⁺	224⁻ (Y=32)
D(0)[2]										
D(1)	—	48	$Sb_2Mn_2M_{12}$	(40⁺)	M_{16}	(32⁺)	$Mn_6M_4X_6$	(40⁺)	112⁺	112⁻ (Y=16)
D(2)	—	72	$Sb_4Mn_2M_{18}$	(62⁺)	M_{24}	(48⁺)	$Mn_{12}M_2X_{10}$	(60⁺)	170⁺	168⁻ (Y=24)
D(3)	blatterite	96	$Sb_6Mn_2M_{24}$	(84⁺)	M_{32}	(64⁺)	$Mn_{16}M_2X_{14}$	(80⁺)	228⁺	224⁻ (Y=32)
B(1)D(2)	—	96	$Sb_4Mn_6M_{22}$	(82⁺)	M_{32}	(64⁺)	$Mn_{18}M_2X_{14}$	(80⁺)	226⁺	224⁻ (Y=32)
D(1)B(2)	—	96	$Sb_2Mn_{10}M_{20}$	(80⁺)	M_{32}	(64⁺)	$Mn_{18}M_2X_{14}$	(80⁺)	224⁺	224⁻ (Y=32)

[1] designation for type of F-wall; [2] hypothetical derivative structure unlikely to exist, B(0) = D(0); [3] number of octahedra in the unit cell; [4] $Sb = Sb^{5+}$; $Mn = Mn^{3+}$; $M = Mn^{2+}$,Mg; $X = Mn^{2+}$,Mg

Thus for structure $D(1)$ (Table 10), the structural formula is

$Sb\, Mn_5\, M_{15}\, X_3\, (BO_3)_8\, O_{16}$.
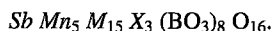
These minerals also contain Fe^{3+}; this may substitute for Mn^{3+} or for (Mn^{2+},Mg), and we should allow for both possibilities when writing formulae. Thus $Sb = Sb^{5+}$, $Mn = (Mn^{3+},Fe^{3+})$, $M + X = [(Mn,Mg), Fe^{3+},\square]$, and the corresponding chemical formula of structure $D(1)$ is

$Sb^{5+} (Mn^{3+},Fe^{3+})_5 [(Mn^{2+},Mg)_x Fe^{3+}_y \square_z]_{\Sigma18}$ $(BO_3)_8 O_{16}$.
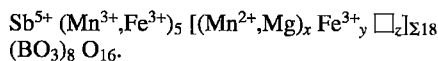
Electroneutrality requires that the sum of the positive charge of the species within the square brackets be 36^+. This means that $2x + 3y = 36$ and also $x + y + z = 18$. Rearranging these equations gives $y = 2z$, and hence we can write the above formula as

$Sb^{5+} (Mn^{3+},Fe^{3+})_5 [(Mn^{2+},Mg)_x Fe^{3+}_y \square_{y/2}]_{\Sigma18}$ $(BO_3)_8 O_{16}$.
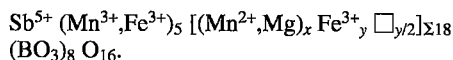
The corresponding formula for structure $D(2)$ and blatterite are shown in Table 11; these formulae may

also be generalized, as shown for $D(N)$ (Table 11). The interesting feature of these formulae is that $D(1)$ does not need to have vacancies present, whereas $D(2)$ and higher values of N *require* vacancies for electroneutrality. Thus examining the most general formula for blatterite (Table 11), if there is no Fe^{3+} at the M or X sites (*i.e.*, $y = 0$), then the vacancy content is $1 + y/2 = 1\ \square\ pfu$, as found in this study. This result is also in accord with our assignment of Fe^{3+} to the Mn sites rather than the M or X sites. According to this general formula, Fe^{3+} substitution at M or X will lead to additional vacancies (presumably at the X sites), but none of the currently available chemical data suggest that this is the case. As the minimum vacancy content of blatterite is $1\ \square\ pfu$, we have written the formula as shown in Table 7. According to the small amount of available data, Fe^{3+} occurs at the Mn sites rather than the M sites.

The B structures

Following the method outlined in the previous section, we may also write the formulae of the B structure in a similar way (Table 11). A key difference between the B and D structures emerges here. The amount of vacancy at the X (and M sites) is independent of the

TABLE 11. GENERAL FORMULAE FOR THE 6Å Mn^{3+}-BEARING ZIGZAG BORATES

D(1)	Sb^{5+}	Mn^{3+}_5	$[(Mn^{2+},Mg)_x Fe^{3+}_y \square_{y/2}]_{\Sigma=18}$	$(BO_3)_8$	O_{16}
D(2)	Sb^{5+}_2	Mn^{3+}_7	$[(Mn^{2+},Mg)_x Fe^{3+}_y \square_{1/2+y/2}]_{\Sigma=27}$	$(BO_3)_{12}$	O_{24}
blatterite	Sb^{5+}_3	Mn^{3+}_9	$[(Mn^{2+},Mg)_x Fe^{3+}_y \square_{1+y/2}]_{\Sigma=36}$	$(BO_3)_{16}$	O_{32}
D(N)	Sb^{5+}_n	Mn^{3+}_{2n+3}	$[(Mn^{2+},Mg)_x Fe^{3+}_y \square_{(n-1+y)/2}]_{\Sigma=9(n+1)}$	$(BO_3)_{4(n+1)}$	$O_{8(n+1)}$
orthopinaklolite		Mn^{3+}_7	$[(Mn^{2+},Mg)_x Fe^{3+}_y \square_{1/2(y-1)}]_{\Sigma=17}$	$(BO_3)_8$	O_{16}
takéuchiite		Mn^{3+}_{11}	$[(Mn^{2+},Mg)_x Fe^{3+}_y \square_{1/2(y-1)}]_{\Sigma=25}$	$(BO_3)_{12}$	O_{24}
B(3)		Mn^{3+}_{15}	$[(Mn^{2+},Mg)_x Fe^{3+}_y \square_{1/2(y-1)}]_{\Sigma=33}$	$(BO_3)_{16}$	O_{32}
B(N)		Mn^{3+}_{4n+3}	$[(Mn^{2+},Mg)_x Fe^{3+}_y \square_{1/2(y-1)}]_{\Sigma=8(n+1)+1}$	$(BO_3)_{4(n+1)}$	$O_{8(n+1)}$

value of N in the general formula (Table 11). Moreover, Fe^{3+} is an essential constituent of this part of the structure. Even if there are no vacancies in each of these structures, they all contain essential Fe^{3+}: 1 *apfu*. If vacancies are to be incorporated at the X sites, as required by the stereochemistry of this part of the structure (see discussion above), then Fe^{3+} must substitute at the M or X sites *in addition to the 1 apfu* required for electroneutrality in the (hypothetical) absence of any vacancies.

For the B structures, $y = 1 + 2z$, where y and z are the amounts of Fe^{3+} and $\square$ in the formulae (Table 11). For orthopinakiolite, Takéuchi *et al.* (1978) reported 0.41 $\square$ *pfu*. According to the above equation, this should correspond to 1.82 Fe^{3+} *apfu*; Takéuchi *et al.* (1978) reported 1.76 Fe^{3+} *apfu*, in excellent accord with the general formula. For takéuchiite, Bovin & O'Keeffe (1980) did not report any vacancy. However, recasting their analytical data as oxides and using the $Mn^{3+}:Mn^{2+}$ ratio indicated by our general formula for takéuchiite in Table 11, we get the chemical composition and unit formula of Table 12. Recasting the formula as given in Table 11, we get $Mn^{3+}_{11.00}$ [$(Mg,Mn^{2+})_{21.79}$ $Fe^{3+}_{2.27}$ $Ti^{4+}_{0.15}$ $\square_{0.79}$]$_{\Sigma 25}$ $(BO_3)_{12}$ O_{24}.

Inspection of Table 11 indicates that the amount of vacancy is given by $\frac{1}{2}(y - 1)$, where y is the amount of trivalent cations within the square brackets. Allowing for the Ti^{4+} content, $y = 2.27 + 0.15 \times 2 = 2.57$. Thus the predicted vacancy content is $\frac{1}{2}(2.57 - 1) = 0.79$ $\square$ *pfu*, in exact agreement with that predicted by the general formula. We emphasize here that incorporation of $\square$ is driven by the bond-valence requirements of the meridional anions of the (MnO_6) octahedra, and that Fe^{3+} and Ti are incorporated at the M or X sites to maintain electroneutrality.

Speculations about the structure of chestermanite

Chestermanite was reported as a new mineral by Erd & Foord (1987), and the structure was reported by Alfredsson *et al.* (1991). The latter authors reported chestermanite to be isotypic with orthopinakiolite. However, they refined a substructure with c (chestermanite) $\approx \frac{1}{2} c$ (orthopinakiolite) and space-group symmetry *Pbam* (rather than *Pnnm* for orthopinakiolite). Alfredsson *et al.* (1991) observed diffraction maxima violating space-group symmetry *Pbam*, but suggested that these diffraction maxima "can probably be ascribed to dynamical (multiple) scattering effects". Chestermanite is rather a curious zigzag borate as it has virtually no Mn^{3+} and yet seems to belong to this group of structures. Table 12 gives the chemical composition of chestermanite and the formula calculated on the basis of 40 atoms of oxygen. In the formula, Sb^{5+} is approximately equal to 1 *apfu*, M^{3+}, to 5 *apfu*, and M^{2+}, to 18 *apfu*. Written in this way, the formula corresponds almost exactly to the D(1) structure of Table 11. There is no vacancy associated with the divalent cations of the formula [*i.e.*, $y = 0$ in the D(1) formula of Table 11].

TABLE 12. CHEMICAL COMPOSITIONS AND FORMULAE OF TAKÉUCHIITE AND CHESTERMANITE

	Takéuchiite*	Chestermanite*	Takéuchiite**		Chestermanite**	
Sb_2O_5	–	10.30	Mn^{3+}	11.00	Sb^{5+}	0.98
Al_2O_3	–	5.30	Mn^{2+}	3.10	Fe^{3+}	3.07
Mn_2O_3	35.56	0.11	Mg	18.69	Al	1.59
Fe_2O_3	7.43	16.00	Sum	21.79	Mn^{3+}	0.02
MnO	8.99	–			Ti^{4+}	0.15
MgO	30.84	48.00	Fe^{3+}	2.27	Mg	0.17
TiO_2	0.50	0.80	Ti^{4+}	0.15	Sum	5.00
$(B_2O_3)†$	17.10	18.19				
Sum	100.42	98.70	B	12	Mg	18.06
					B	8

* Taken from Bovin & O'Keeffe (1980); the Mn^{3+}/Mn^{2+} ratio is derived from the ideal formula of Table 11.
** Calculated on the basis of 60 O-atoms.
⁺ Taken from Erd & Foord (1987).
⁺⁺ Calculated on the basis of 40 O-atoms.
† B_2O_3 calculated for 12 and 8 B *apfu*, respectively.

However, the above discussion indicates that the D(1) structure does not require any vacancy (whereas all the other D structures do require vacancies to be present). Orthopinakiolite, the supposed isotype of chestermanite, is not a D structure, and hence does not contain significant Sb^{5+}. These arguments suggest that chestermanite is actually a D(1) structure rather than an orthopinakiolite isotype. Also, as discussed above, the presence of vacancies at the X sites is linked to the occurrence of Mn^{3+} in these structures. Thus it may be no accident that the only structure variant that does not require vacancies for electroneutrality is the only mineral in the group that does not contain Mn^{3+} as an essential constituent.

Additional TEM and single-crystal study will surely result in the discovery of additional derivative structures in this complex group of minerals.

REFERENCES

ALFREDSSON, V., BOVIN, J.-O., NORRESTAM, R. & TERASAKI, O. (1991): The structure of the mineral chestermanite, $Mg_{2.25}Al_{0.16}Fe_{0.43}Ti_{0.02}Sb_{0.13}O_2BO_3$. A combined single-crystal X-ray and HREM study. *Acta Chem. Scand.* **45**, 797-804.

BONAZZI, P. & MENCHETTI, S. (1989): Contribution to the crystal chemistry of the minerals of the ludwigite – vonsenite series. *Neues Jahrb. Mineral., Monatsh.*, 69-83.

BOVIN, J.-O., CARLSSON, A., SJÖVALL, R., THOMASSON, R., NORRESTAM, R. & SØTOFTE, I. (1996): The crystal structure of a blatterite mineral, $Mg_{1.33}Mn_{1.44}Fe_{0.05}Sb_{0.17}O_2BO_3$, a combined single crystal X-ray and HREM study. *Z. Kristallogr.* **211**, 440-448.

————— & O'KEEFFE, M. (1980): Takéuchiite, a new oxyborate mineral from Långban, Sweden. *Am. Mineral.* **65**, 1130-1133.

BROWN, I.D. (1981): The bond-valence method: an empirical approach to chemical structure and bonding. *In* Structure and Bonding in Crystals II (M. O'Keeffe and A. Navrotsky, eds.). Academic Press, New York, N.Y. (1-30).

BURNS, P.C., COOPER, M.A. & HAWTHORNE, F.C. (1994): Jahn–Teller distorted $Mn^{3+}O_6$ octahedra in fredriksssonite, the fourth polymorph of $Mg_2Mn^{3+}(BO_3)O_2$. *Can. Mineral.* **32**, 397-403.

—————, GRICE, J.D. & HAWTHORNE, F.C. (1995): Borate minerals. I. Polyhedral clusters and fundamental building blocks. *Can. Mineral.* **33**, 1131-1151.

————— & HAWTHORNE, F.C. (1993a): Hydrogen bonding in meyerhofferite: an X-ray and structure energy study. *Can. Mineral.* **31**, 305-312.

————— & ————— (1993b): Hydrogen bonding in colemanite: an X-ray and structure energy study. *Can. Mineral.* **31**, 297-304.

————— & ————— (1994a): Structure and hydrogen bonding in preobrazhenskite, a complex heteropolyhedral borate. *Can. Mineral.* **32**, 387-396.

————— & ————— (1994b): Structure and hydrogen bonding in inderborite, a heteropolyhedral sheet structure. *Can. Mineral.* **32**, 533-539.

————— & ————— (1994c): Refinement of the structure of hilgardite-1A. *Acta Crystallogr.* **C50**, 653-655.

————— & ————— (1994d): Kaliborite, an example of a crystallographically symmetrical hydrogen bond. *Can. Mineral.* **32**, 885-894.

————— & ————— (1994e): Hydrogen bonding in tunellite. *Can. Mineral.* **32**, 895-902.

————— & ————— (1995): Hydrogen bonding in borcarite, an unusual borate–carbonate mineral. *Mineral. Mag.* **59**, 297-304.

—————, ————— & STIRLING, J.A.R. (1992): Trembathite, $(Mg,Fe)_3B_7O_{13}Cl$, a new borate mineral from the Salt Springs potash deposit, Sussex, New Brunswick. *Can. Mineral.* **30**, 445-448.

COOPER, M., HAWTHORNE, F.C., NOVAK, M. & TAYLOR, M.C. (1994): The crystal structure of tusionite, $Mn^{2+}Sn^{4+}(BO_3)_2$, a dolomite-structure borate. *Can. Mineral.* **32**, 903-907.

DE WAAL, S.A., VILJOEN, E.A. & CALK, L.C. (1974): Nickel minerals from Barberton, South Africa. VII. Bonaccordite, the nickel analogue of ludwigite. *Trans. Geol. Soc. S. Africa* **77**, 373.

ERD, R.C. & FOORD, E.E. (1988): Chestermanite, a new member of the ludwigite–pinakiolite group from Fresno County, California. *Can. Mineral.* **26**, 911-916.

FLEISCHER, M. & MANDARINO, J.A. (1995): *Glossary of Mineral Species.* The Mineralogical Record, Tucson, Arizona.

HAWTHORNE, F.C. (1978): The crystal chemistry of the amphiboles. VI. The stereochemistry of the octahedral strip. *Can. Mineral.* **16**, 37-52.

————— (1994): Structural aspects of oxides and oxysalt crystals. *Acta Crystallogr.* **50**, 481-510.

—————, BURNS, P.C. & GRICE, J.D. (1996): The crystal chemistry of boron. *Rev. Mineral.* **33**, 41-115.

————— & GRICE, J.D. (1990): Crystal structure analysis as a chemical analytical method: application to light elements. *Can. Mineral.* **28**, 693-702.

JAHN, H.A. & TELLER, E. (1937): Stability of polyatomic molecules in degenerate electronic states. *Proc. R. Soc., Ser. A* **161**, 220-236.

KONEV, A.A., LEBEDEVA, V.S., KASHAEV, A.A. & USCHAPOV-SKAYA, Z.F. (1970): Azoproite, a new mineral of the ludwigite group. *Zap. Vses. Mineral. Obshchest.* **99**, 225-231.

KONNERT, J.A., APPLEMAN, D.E. & CLARK, J.R. (1976): Crystal structure and cation distribution of hulsite, a tin–iron borate. *Am. Mineral.* **61**, 116-122.

MOORE, P.B. & ARAKI, T. (1974): Pinakiolite, $Mg_2Mn^{3+}O_2$ $[BO_3]$; warwickite, $Mg(Mg_{0.5}Ti_{0.5})O[BO_3]$; wightmanite, $Mg_3(O)(OH)_5[BO_3]\cdot nH_2O$: crystal chemistry of complex 3 Å wallpaper structures. *Am. Mineral.* **59**, 985-1004.

NORRESTAM, R. & BOVIN, J.-O. (1987): The crystal structure of takéuchiite, $Mg_{1.71}Mn_{1.29}BO_5$, a combined single crystal X-ray and HRTEM study. *Z. Kristallogr.* **181**, 135-149.

POUCHOU, J.-L. & PICHOIR, F. (1984): A new model for quantitative analysis. I. Application to the analysis of homogeneous samples. *Recherche Aérospatiale* **3**, 13-38.

————— & ————— (1985): "PAP" .(Z) procedure for improved quantitative microanalysis. *Microbeam Anal.*, 104-106.

RAADE, G., MLADECK, M.H., DIN, V.K., CRIDDLE, A.J. & STANLEY, C.J. (1988): Blatterite, a new Sb-bearing $Mn^{2+}-Mn^{3+}$ member of the pinakiolite group, from Nordmark, Sweden. *Neues Jahrb. Mineral., Monatsh.*, 121-136.

SHANNON, R.D., GUMERMAN, P.S. & CHENAVAS, J. (1975): Effect of octahedral distortion on mean Mn^{3+}–O distances. *Am. Mineral.* **60**, 714-716.

SWINNEA, J.S. & STEINFINK, H. (1983): Crystal structure and Mössbauer spectrum of vonsenite, 2FeO·FeBO₃. *Am. Mineral.* **68**, 827-832.

TAKÉUCHI, Y. (1978): 'Tropochemical twinning': a mechanism of building complex structures. *Recent Progr. Natur. Sci. Jap.* **3**, 153-181.

_____ (1997): *Tropochemical Cell-Twinning: a Structure-Building Mechanism in Crystalline Solids.* Terra Scientific Publishing, Tokyo, Japan.

_____, HAGA, N., KATO, T. & MIURA, Y. (1978): Ortho-pinakiolite, $Me_{2.95}O_2[BO_3]$: its crystal structure and relationship to pinakiolite, $Me_{2.90}O_2[BO_3]$. *Can. Mineral.* **16**, 475-485.

YANG, GUANGMING, PENG, ZHIZHONG & PAN, ZHAOLU (1985): Magnesiohulsite: a new tin-rich borate mineral. *Acta Mineral. Sinica* **5**, 97-101 (in Chinese with English abstr.).